

Article

Automated Solar PV Simulation System Supported by DC–DC Power Converters

Armando Cordeiro ^{1,2,3,*}, Miguel Chaves ^{1,2}, Paulo Gâmbao ^{1,2}, Filipe Barata ¹, Pedro Fonte ^{1,3}, Hélio Lopes ¹, Vítor Fernão Pires ^{2,4}, Daniel Foito ^{4,5}, Tito G. Amaral ⁴ and João Francisco Martins ⁵

- ¹ Electrical Engineering Energy and Automation Department (DEEEA), Instituto Superior de Engenharia de Lisboa (ISEL), Instituto Politécnico de Lisboa (IPL), Estrada de Benfica 529, 1549-020 Lisboa, Portugal
- ² Instituto de Engenharia de Sistemas e Computadores: Investigação e Desenvolvimento em Lisboa (INESC-ID Lisbon), 1000-029 Lisboa, Portugal
- ³ Low Carbon Energy Conversion (LCEC), Rua Conselheiro Emídio Navarro 1, 1959-007 Lisboa, Portugal
- ⁴ Sustainable Research and Development Center (SustainRD), ESTSetúbal, Polytechnic Institute of Setúbal, 2914-508 Setúbal, Portugal
- ⁵ Centre of Technology and Systems (CTS), Instituto de Desenvolvimento de Novas Tecnologias (UNINONA), Electrical Engineering Department (DEE), Faculdade de Ciências e Tecnologia (FCT), Universidade Nova de Lisboa (UNL), 2829-516 Caparica, Portugal
- * Correspondence: armando.cordeiro@isiel.pt

Abstract: Solar photovoltaic simulators are valuable tools for the design and evaluation of several components of photovoltaic systems. They can also be used for several purposes, such as educational objectives regarding operation principles, control strategies, efficiency, maintenance, and other aspects. This paper presents an automated solar photovoltaic simulation system with the capability to generate automated tests considering different parameters of solar photovoltaic panels and different operation conditions. The proposed simulator is composed of three buck-boost DC–DC power converters controlled in such a way that will behave similarly to solar photovoltaic panels. It allows to introduce additional variable loads and maximum power point tracker algorithms similar to real systems. Some converters are controlled by a DSP microcontroller connected to a single programmable logic controller which generates the automated tests. Thus, using the presented solution, it is possible to implement the *I-V* and *P-V* characteristic curves of solar photovoltaic panels and evaluate different maximum power point tracker algorithms considering different meteorological conditions and load variations, being a useful tool to teach subjects related to renewable energy sources and related applications. Several simulation results using Matlab/Simulink and experimental results are presented to validate the operation of the proposed solution. Experimental results achieve a ripple between 2% and 5% of the desired average current in MPP conditions.

Keywords: PV simulator; sliding mode controller; buck-boost DC–DC converter; programmable logic controller; SCADA system



Citation: Cordeiro, A.; Chaves, M.; Gâmbao, P.; Barata, F.; Fonte, P.; Lopes, H.; Pires, V.F.; Foito, D.; Amaral, T.G.; Martins, J.F. Automated Solar PV Simulation System Supported by DC–DC Power Converters. *Designs* **2023**, *7*, 36. <https://doi.org/10.3390/designs7020036>

Academic Editors: Mohsin Jamil, Yuanmao Ye and Tomasz Pajchrowski

Received: 11 January 2023

Revised: 11 February 2023

Accepted: 21 February 2023

Published: 1 March 2023



Copyright: © 2023 by the authors. Licensee MDPI, Basel, Switzerland. This article is an open access article distributed under the terms and conditions of the Creative Commons Attribution (CC BY) license (<https://creativecommons.org/licenses/by/4.0/>).

1. Introduction

In recent years, there has been widespread concern about climate change as a result of the excessive amount of carbon dioxide in the atmosphere disturbing the greenhouse effect with impacts on global warming [1]. To mitigate this global problem, several countries and organizations are now promoting a smooth transition from fossil fuel energy sources to clean or reduced ecological footprint energy sources. This transition can be seen in different sectors from manufacturing to utilities, transportation, construction, and buildings. It is interesting to realize that climate changes are most likely a consequence of the technological advances achieved over the last century, and now, new technological advances are necessary to overcome the problems generated by themselves. According to some relevant reports [2,3], the use of renewable energy sources, especially wind and

solar photovoltaic (*SPV*) panels, is increasing worldwide. Investments in renewable energy sources are continuously breaking records, helping to supply electricity to public and private installations. Energy prices are also contributing to many companies and individuals becoming prosumers using mostly private *SPV* generators. According to an International Energy Agency [2] report, *SPV* and wind contributed around two-thirds of renewables' growth in 2021. China alone achieved almost half of the global increase in renewable electricity in 2021, followed by the United States, the European Union, and India. In 2021, *SPV* electricity generation rose almost 145 TWh, or almost 18%, approaching 1000 TWh. Such reports reveal that *SPV* plays an important role in global energy production. This has been boosted thanks to lower production costs as a consequence of massive production, propelled by the expansion of new markets supported by governmental policies.

Nevertheless, there are always new aspects to be investigated and improved in the design of components and raw materials for *PV* systems. To continuously push new developments and additional *SPV* installations, it is also necessary to teach operation principles, control strategies, handling, efficiency, and maintenance aspects to easily integrate and exploit them in both on-grid and off-grid applications. In this sense, to encourage the development and installation of *SPV* panels, it is also necessary to create new tools designed to train technicians and young engineers [4–7].

There are usually some constraints regarding testing *SPV* panels. Some of them are related to the variability of the operating conditions (as irradiation and temperature are not steady over the day), and the relative position between the sun and solar panels changes constantly [8]. For academic and research purposes, field tests of *SPV* panels are usually quite costly and heavily depend on weather conditions. For this reason, several low-cost tools and methods developed to simulate the behavior of the panels have been proposed in the literature. Most tools to simulate *SPV* panels are software-based solutions dedicated to theoretical models. Some of the most common models are the voltage–temperature simulation algorithms [9], end-to-end differentiable simulator [10], seven-parameter model [11], one-diode equivalent circuit model [12,13], dual-diode model [14], or four-diode model [15]. Other simulation tools are dedicated to the research of *PV* panels regarding operational data for the reliability or fault-tolerant analysis and improvement [16]. Some authors propose solutions using a constant *DC* power supply and adjustable loads to achieve different operational conditions [17]. An *SPV* simulator using a nonlinear *DC* power source for high-power application was also suggested in [18]. There are also hardware-based solutions based on high-frequency switching power converters, such as those proposed by [19–21]. Other low-cost solutions mixing hardware and software were also developed. Some of these solutions are programmable microcontroller-based solutions using different *DC–DC* converters, such as buck, boost, or buck-boost [22–25]. Despite the features of these solutions, most of them are not flexible enough to accept different *SPV* module types or are not designed to redefine the operational conditions (such as temperature and/or solar irradiance or are not designed to select and implement diverse *MPPT* (maximum power point tracker) algorithms when connected to on-grid and off-grid applications.

This paper presents a complete *SPV* simulator based on three buck–boost *DC–DC* power converters, each one performing a different function. The first one is used to simulate the *SPV* panel, the second one is used to test the desired *MPPT* algorithm, and the third one is used to perform an automatic load variation. A complete laboratorial prototype to simulate *SPV* systems up to 365 W was developed for this purpose. The main core of this system is a *DSP* microcontroller and a programmable logic controller (*PLC*), which, combined with the three *DC–DC* converters, makes possible the performance evaluation of distinct *SPV* panels, *MPPT* algorithms, temperature, solar irradiance, and load variation. Using the proposed topologies and the automatic control strategy for the *DC–DC* converters, a fast dynamic change was obtained in the *SPV* simulator system according to the desired variations, reaching a good performance in distinct load conditions and with several *MPPT* algorithms. The originality of the proposed system is to automatically replicate the typical *PV* panels' characteristic curves, obtained from manufacture manuals while testing

different MPPT algorithms. The main contribution of this paper is the development and creation of new tools designed to train technicians and young engineers, giving them the chance of testing the concepts and operation of SPV systems, without having the costs involved in the acquisition of all the necessary real equipment. This can be a very useful tool for laboratories, technical schools, and SPV industries. Further, as this project involves industrial equipment, it shows how to integrate SPV systems with the aim of spreading renewable energy sources while contributing to demonstrating how-to-use examples.

2. Description of the Proposed System

The main elements of this system are three buck–boost DC–DC converters, a regulated DC power supply, a DSP microcontroller, a PLC linked to supervisory control and data acquisition (SCADA) software, analog signal conditioning boards (current and voltage), a couple of analog sliding mode circuits, a PWM (pulse width modulation) modulator circuit, and an RL load. The system was developed to work in two separate modes. The first mode (mode I), or SPV panel mode, and the second mode (mode II), or MPPT test mode. Despite the same topology and components, the first and third DC–DC converters will operate in Buck mode and the second DC–DC converter will operate in Boost mode (see Figure 1).

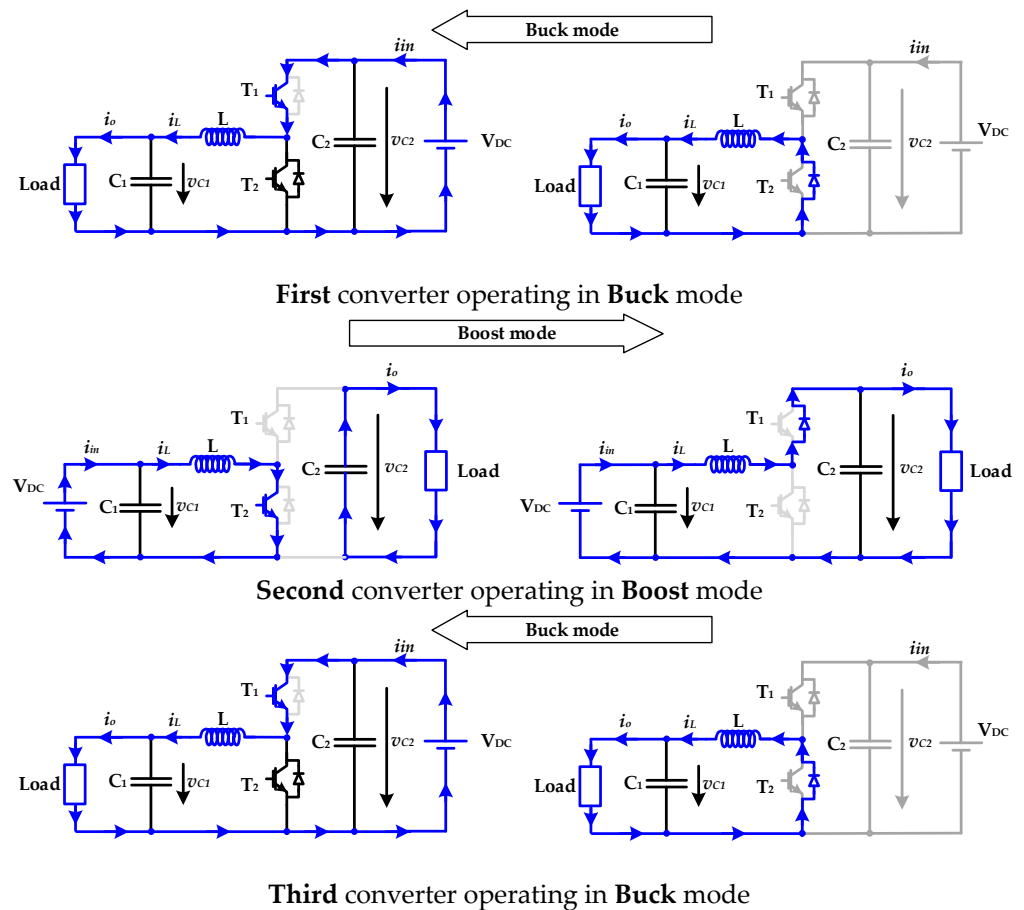


Figure 1. Description of the functionality of each DC–DC converter. Despite the same topology and components, each one will perform a different function.

Table 1 summarizes the operation modes of each converter.

Table 1. Summary of the different operation modes and converter’s functionality.

Operation Mode	Converter Used	Topology	Description
Mode I (SPV panel mode)	1st converter connected in series with ...	Buck mode	Simulate the I-V PV curves
	3rd converter	Buck mode	Simulate a variable load (Fixed load with variable voltage)
Mode II (MPPT test mode)	1st converter connected in series with ...	Buck mode	Simulate the I-V PV characteristics
	2nd converter connected in series with ...	Boost mode	Simulate the MPPT algorithm
	3rd converter	Buck mode	Simulate a variable load (Fixed load with variable voltage)

2.1. Mode I—Test and Emulate Characteristic I-V Curves

Figure 2 presents the general block diagram of mode I. Mode I is exclusively devoted to testing and emulating the characteristic *I-V* curves of the panel according to parameters provided by the manufacturer datasheet manual. Applying these parameters to an *SPV* model and considering different temperature reference and solar irradiance values, along with a variable load, it is possible to obtain the expected voltage and current of the *SPV* panel. In this mode are used only two *DC-DC* buck-boost converters (both in Buck operation mode). In this case, the first *DC-DC* converter simulates the *SPV* current and voltage panel, and the other *DC-DC* converter is used to perform load variation through *PWM* over a fixed *RL* load. This mode requires different stages to provide the correct operation. The first stage consists of adjusting the regulated *DC* power supply, the converter of which simulates the *SPV* panel. The next stage involves introducing the *SPV* panel parameters, the required temperature reference, and solar irradiance values in the *SCADA* software. Notice that the *SCADA* software was designed to accept *SPV* panels up to 365 W. Additionally, the *SCADA* software has the same *SPV* model of the *DSP* microcontroller and rejects data if they are out of range, avoiding creating problems in the controller and *DC-DC* converters. In this sense, the system is able to specify up to 15 variable load percentage values (to simulate the load variation at the terminals of the panel).

After validating the introduction of all the necessary information, the *SCADA* software will send the introduced data to the connected *PLC* using an Ethernet connection with Modbus TCP/IP protocol. The *PLC* collects all the information and sends the necessary data to the *DSP* device using a serial *RS232-C* interface. The information about load variation is used internally by the *PLC* to control the *PWM* of the third *DC-DC* converter (load regulator, see Figure 2). After processing all the information, the *PLC* starts the simulation of the *SPV* panel *I-V* curves. The *PLC* program is now able to automatically change the pre-specified step load reference 15 times during this process. During this process, the *PLC* records in the internal memory register the current and voltage feedback received by the analog interface. As current and voltage are continuously changing in the real *DC-DC* converters, the *PLC* also calculates the average values during each step. The progress of the simulations is continuously displayed in proper screen layouts using trend charts in the *SCADA* software. A flowchart of this operation mode is available in the experimental results sections among more details about software and hardware.

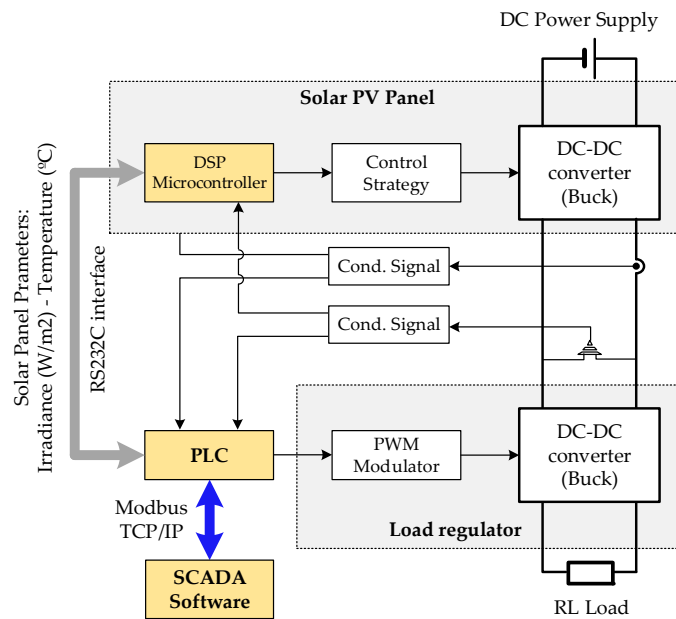


Figure 2. General block diagram of test panel mode (mode I).

2.2. Mode II—MPPT Test Mode

The operational diagram block of mode II (or *MPPT* test mode) can be seen in Figure 3. This simulation mode introduces some additional features to mode I to test the *MPPT* control algorithm adopted and assess the produced power in several load conditions. For educational purposes, this provides the possibility to understand how to obtain the maximum power of an *SPV* (although not connected to the grid). In this simulation mode an additional *DC-DC* buck–boost converter is used, operating now in Boost mode (as described in Figure 3).

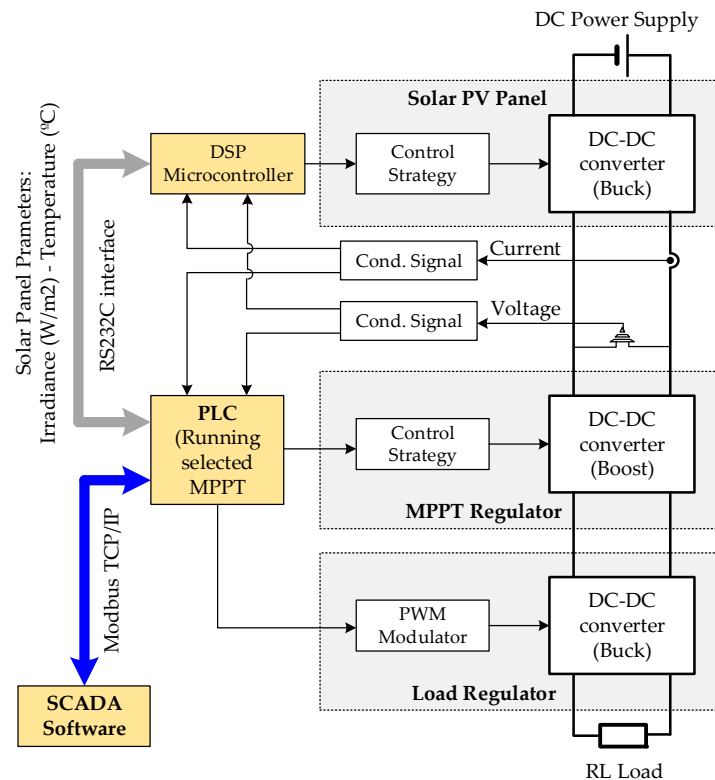


Figure 3. General block diagram of the MPPT test mode (mode II).

The procedures to operate in mode II are similar to mode I. Nevertheless, in this mode, in addition to all the introduced parameters specified in mode I, it is also necessary to select the preferred *MPPT* algorithm. In the proposed system, only two well-known *MPPT* techniques were effectively implemented, namely, hill climbing (HC) and perturb and observe (*P&O*) [26,27]. Theoretically, other *MPPT* techniques [28,29] can be implemented, although some of them are usually complex and require high-speed processors, which might not be compatible with the *PLC* adopted. An article presenting a modified fuzzy logic control algorithm for the extraction of maximum power through PV systems under severe climatic drifts can be found in [30]. Additionally, an *MPPT* algorithm using a modified incremental conductance technique in a grid-connected PV array is presented in [31]. The chosen techniques were selected due to their simplicity and efficiency for uniform solar irradiation conditions as the *SPV* will create only one global *MPP* in such conditions. A flowchart of this operation mode is available in the experimental results sections among more details about software and hardware.

2.3. Converters Design

In this work, it was adopted a unique *PCB* board design with the classic buck–boost *DC–DC* power converter. The design allows to choose the desired Buck or Boost connection. The simplified diagram of this classic topology can be seen in Figure 4. Thus, by connecting this dual *DC–DC* converter from the left side to the right side (switching on *T2* and turning off *T1*), the converter operates in Boost mode (Figure 4a,b). Reversing the load and power supply position operates in Buck mode (switching on *T1* and turning off *T2*) (Figure 4c,d). Other topologies can be used with higher voltage gain and other characteristics, depending on the desired requirements. In the proposed work, it was considered that the classic buck–boost *DC–DC* converter was adequate for this purpose, as demonstrated by some experimental results.

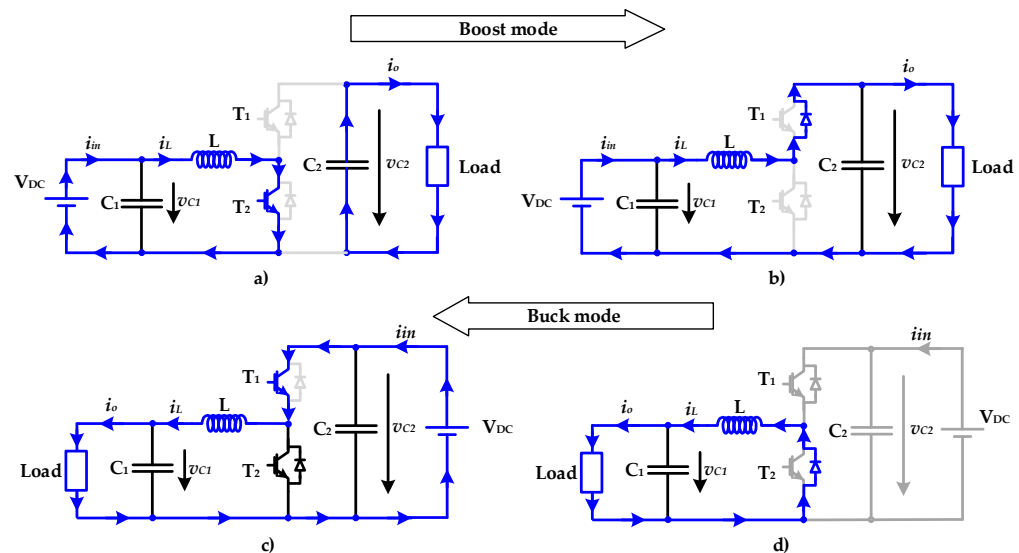


Figure 4. Classic buck–boost *DC–DC* topology adopted; (a,b) Boost mode connection; (c,d) Buck mode connection.

The following sizing calculations, based on [32], are designed in two different conditions, the Buck and Boost modes. Despite the topology being the same, they were designed in different situations. The results achieve different minimum values for the output capacitor, but, in order to standardize the converter, the same components were adopted. The solution was designed to a maximum output power of 365W [33] using the maximum power of a connected *SPV* panel as described in the next table.

Designing the converter components in Buck mode (topology used as *SPV* simulator) requires knowing three parameters:

- Input voltage V_{DC} ;
- Minimum output voltage $V_{OUT(\min)}$;
- Maximum output current $I_{OUT(\max)}$.

The first step is to calculate the maximum current flowing through the semiconductor, so it is necessary to know the maximum duty cycle in operation. In Equation (1), the efficiency is considered to obtain a more realistic duty cycle value. An efficiency value of $\eta = 90\%$ was considered as a worst-case scenario value for this buck converter. The $V_{OUT(\min)}$ value considered in this condition is the voltage at the *MPP* of the *SPV* panel presented in Table 2. It was also considered an input voltage $V_{DC} = 60$ V.

$$\delta_1 = \frac{V_{OUT(\min)}}{\eta V_{DC}} = \frac{33.6}{0.9 \times 60} \approx 0.62 \tag{1}$$

Table 2. Characteristics of an *SPV* panel with the maximum power of the proposed converter (in *STC*) [32].

Parameter	Value
Voltage at <i>MPP</i>	33.6 V
Current at <i>MPP</i>	10.75 A
Power at <i>MPP</i>	365 W
Open-circuit voltage	41.13 V
Short-circuit current	11.3 A

With the duty cycle, it is now possible to obtain the inductor current ripple ΔI_L , assuming a maximum switching frequency of $f_s = 20$ kHz (this is the maximum frequency that the *DSP* device achieves) and an inductor value of $L = 1$ mH. The inductor current ripple is given by Equation (2).

$$\Delta I_L = \frac{(V_{DC} - V_{OUT})\delta_1}{L f_s} = \frac{(60 - 33.6) \times 0.62}{1 \times 10^{-3} \times 20 \times 10^3} = 0.81\text{A} \tag{2}$$

Knowing the *MPP* current (maximum current of the converter $I_{OUT(\max)}$) of the *SPV* panel, it is possible to calculate the peak current that the power semiconductor T1 and inductor L have to withstand, as per Equation (3).

$$I_{L(\max)} = \frac{\Delta I_L}{2} + I_{OUT(\max)} = \frac{0.81}{2} + 10.75 \approx 11.16\text{A} \tag{3}$$

In this mode, the power semiconductor T1 must withstand an average value given by (4).

$$I_{T1(av)} = I_{OUT(\max)}\delta_1 \approx 6.66\text{A} \tag{4}$$

Additionally, in this operation mode, the freewheeling diode $D2$ must withstand an average value given by (5).

$$I_{D2(av)} = I_{OUT(\max)}(1 - \delta_1) \approx 4.08\text{A} \tag{5}$$

The minimum output capacitor value C_1 , considering an acceptable voltage ripple ΔV_{OUT} of 0.1V, is obtained using (6).

$$C_1 = \frac{\Delta I_L}{8\Delta V_{OUT}f_s} = \frac{0.81}{8 \times 0.1 \times 20 \times 10^3} \approx 52\mu\text{F} \tag{6}$$

In order to standardize the converter, it was selected as a capacitor of $C_1 = 470 \mu\text{F}$.

The design of the converter components in Boost mode (topology used as *MPPT* regulator) is similar to the previous one. Considering that both converters are connected in series, the average output current of the buck converter is the average input current

of the boost converter around the same operation point. In fact, in the MPPT test mode, the boost converter imposes the current value on the buck converter. Thus, both power semiconductors $T1$ and $T2$ must withstand the same average value, and, consequently, they have similar duty cycles:

$$I_{T2(av)} = I_{T1(av)} \Leftrightarrow I_{OUT}\delta_2 = I_{OUT}(1 - \delta_1) \Leftrightarrow \delta_2 = (1 - \delta_1) \tag{7}$$

In this condition, the output voltage of the boost converter is given by (8), considering again an efficiency value of $\eta = 90\%$.

$$V_{OUT} = \frac{V_{DC(min)}\eta}{(1 - \delta_2)} = \frac{33.6 \times 0.9}{(1 - 0.38)} \approx 49V \tag{8}$$

Calculating the duty cycle in this mode, it is possible to obtain the inductor current ripple ΔI_L , assuming a fixed switching frequency of $f_s = 60$ kHz and an inductor value of $L = 1$ mH. The inductor current ripple in the boost inductor is given by Equation (9).

$$\Delta I_L = \frac{V_{DC(min)}\delta_2}{L f_s} = \frac{33.6 \times 0.38}{1 \times 10^{-3} \times 60 \times 10^3} \approx 0.21A \tag{9}$$

In the above conditions, the peak current that the power semiconductor $T2$ and inductor L have to withstand is given by (10).

$$I_{L(max)} = \frac{\Delta I_L}{2} + I_{OUT(max)} = \frac{0.21}{2} + 10.75 \approx 10.85A \tag{10}$$

Additionally, in this mode, the freewheeling diode $D1$ must withstand an average value of (11).

$$I_{D1(av)} = I_{OUT(max)}(1 - \delta_2) \approx 6.66A \tag{11}$$

The minimum output capacitor value C_2 for the boost converter considering an acceptable voltage ripple ΔV_{OUT} of 0.1 V is given by (12).

$$C_2 = \frac{\Delta I_L}{8\Delta V_{OUT}f_s} = \frac{0.21}{8 \times 0.1 \times 60 \times 10^3} \approx 4.4\mu F \tag{12}$$

In order to standardize the converter, it was selected as a capacitor of $C_2 = 470 \mu F$.

Other strategies to optimize the converter parameters for other topologies can be found in [34].

2.4. Mathematical Model

For this buck–boost converter, a mathematical model can also be developed in which the power semiconductors can be associated with a binary variable. Therefore, the first step for developing the model is to consider the binary variables α_{T_1} and α_{T_2} that are associated with the logical states of transistors T_1 and T_2 with the correspondent antiparallel diodes. These variables are described in (13) and (14)

$$\alpha_{T_1} = \begin{cases} 0, & T_1 \text{ On} \vee D_1 \text{ On} \\ 1, & T_1 \text{ Off} \wedge D_1 \text{ Off} \end{cases} \tag{13}$$

$$\alpha_{T_2} = \begin{cases} 1, & T_2 \text{ On} \vee D_2 \text{ On} \\ 0, & T_2 \text{ Off} \wedge D_2 \text{ Off} \end{cases} \tag{14}$$

Using the referred binary variables, it is now possible to write the converter model as presented in (15) and (16). The model given by (15) is for the Boost mode, whereas the other model (16) is for the Buck mode. In these equations, i_L is the inductor current, i_o is the output current, v_{DC} is the converter input voltage, v_{C1} is the voltage over of the

output converter capacitor (Buck mode), and v_{C2} is the voltage over of the output converter capacitor (Boost mode).

$$\begin{bmatrix} \frac{di_L}{dt} \\ \frac{dv_{C2}}{dt} \end{bmatrix} = \begin{bmatrix} 0 & -\alpha_{T1}\alpha_{T2} \\ \alpha_{T1}\alpha_{T2} & 0 \end{bmatrix} \begin{bmatrix} i_L \\ v_{C2} \end{bmatrix} + \begin{bmatrix} v_{DC} \\ i_o \end{bmatrix} \tag{15}$$

$$\begin{bmatrix} \frac{di_L}{dt} \\ \frac{dv_{C1}}{dt} \end{bmatrix} = \begin{bmatrix} 0 & -1 \\ 1 & 0 \end{bmatrix} \begin{bmatrix} i_L \\ v_{C1} \end{bmatrix} + \begin{bmatrix} \alpha_{T1}\alpha_{T2} \\ -1 \end{bmatrix} \begin{bmatrix} v_{DC} \\ i_o \end{bmatrix} \tag{16}$$

3. SPV Model Adopted

As mentioned in the previous section, the *SVP* panel is simulated using a *DC–DC* buck–boost converter. This *DC–DC* buck–boost converter must operate as a buck converter and must be able to generate an output voltage at the terminals of the output capacitor C_1 , similar to an *SPV* panel (as described in Figure 4c,d). Thus, the control system must be able to impose reference values on the power converter to generate the *I–V* characteristic curve according to the manufacturer’s parameters. The adopted *SPV* model is based on the single-diode model [21] which is one of the most used by academics and industry. This model produces a fairly accurate result and has a low computational cost [35]. This model, instead of a nonlinear *I–V* characteristic approximated as 2^n order line segments, modeled as n diodes connected in parallel (creating a piecewise linear approximation, by sections), proposes a single approximated nonlinear *I–V* characteristic much more accurately. Identifying the five unknown parameters, namely, the ideal *SPV* current I_S , the diode saturation current I_0 , the ideality factor α , the series resistance R_S , and the parallel resistance R_P , the output current–voltage characteristic can be modeled. Figure 5 shows the equivalent circuit of the single-diode model. In this simplified model, I_S represents the ideal photocurrent as a result of a certain light intensity G and cell operating temperature, and the single diode represents the diffusion phenomena where a dark current I_D flows. In this model, I_P represents the current flowing across the parasitic parallel equivalent resistor caused by *P–N* junction imperfections. The serial resistance R_S represents the sum of resistances of the serially connected cell layers and contacts between both ends of the *SPV* panel.

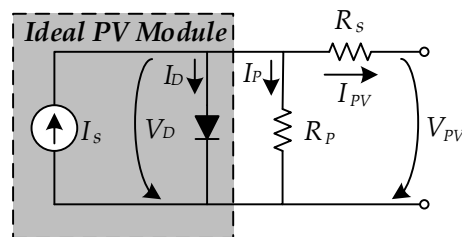


Figure 5. Electric equivalent circuit of an *SPV* module using the single diode model.

The terminal current I_{PV} of the single diode model for the *SPV* panel from Figure 4 can be written by combining all the currents with Equation (17). All these elementary currents will be defined over the next equations.

$$I_{PV} = I_S - I_D - I_P \tag{17}$$

The value of the ideal photocurrent I_S at a temperature reference of $T = 298.15$ K (≈ 25 °C) and an irradiation reference of $G_R = 1000$ W/m² is given by Equation (18). In this equation, I_{SC} is the equivalent short circuit current, and k_i is the short-circuit current coefficient [13].

$$I_S = \frac{[I_{SC} + k_i(T_S - T)]G}{G_R} \tag{18}$$

In this model, the dark current I_D (Equation (19)) depends on several parameters, namely, the reverse saturation current I_0 , the output voltage V_{VP} , the output current I_{PV} , the number of SPV cells connected serially N_s , Shockley’s diode ideality factor α , and the thermal voltage of the SPV module V_T (Equation (20)). In turn, the thermal voltage depends on the Boltzmann constant $k = 1.3806 \times 10^{-23}$ /K, the reference temperature $T = 298.15$ K ($\approx 25^\circ\text{C}$), and the elementary electron charge $q = 1.6022 \times 10^{-19}$ C. The reverse saturation current I_0 is expressed by Equation (21), where $E_g \cong 1.1$ eV is the gap energy for S_i semiconductors, and I_{rr} represents the reverse saturation current at the temperature reference. This current is also dependent on the module cell operating temperature T_S .

$$I_D = I_0 \left(\exp \left(\frac{V_{PV} + I_{PV}R_S}{\alpha N_s V_T} \right) - 1 \right) \tag{19}$$

$$V_T = \frac{kT}{q} \tag{20}$$

$$I_0 = I_{rr} \left(\frac{T_S}{T} \right)^3 \exp \left[\frac{qE_g}{\alpha K} \left(\frac{1}{T} - \frac{1}{T_S} \right) \right] \tag{21}$$

The current flowing across the parasitic parallel resistor is described by Equation (22).

$$I_P = \frac{V_D}{R_P} = \frac{V_{PV} + (R_S I_{PV})}{R_P} \tag{22}$$

Through the arrangement of Equations (17)–(22), it is possible to obtain the estimated value of the output current I_{PV} (Equation (23)).

$$I_{PV} = I_S - I_0 \left(\exp \left(\frac{(V_{PV} + R_S I_{PV})}{\alpha N_s V_T} \right) - 1 \right) - \frac{(V_{PV} + R_S I_{PV})}{R_P} \tag{23}$$

4. Control of the SPV Panel Simulator

The DC–DC buck–boost converter responsible for generating the current–voltage characteristics will be controlled using a sliding mode control technique. The sliding mode control technique presents a fast dynamic reaction and robustness to parameter and load variation [36–38] and has been widely used in numerous renewable energy applications [39,40]. To project this sliding mode controller, it is considered a dynamic model with ideal components, namely, the power transistor, inductor, and capacitors. The switching state of transistor T_1 is described by the time-dependent switching variable λ , as shown by Equation (24) [41].

$$\lambda = \begin{cases} 1, T_1 \rightarrow \text{Turned On} \\ 0, T_1 \rightarrow \text{Turned Off} \end{cases} \tag{24}$$

Examining the correspondence between the voltages and the currents shown in Figure 3c,d, it is possible to obtain a simplified switched model of the DC–DC converter state-space, regarding the controllable variables i_L and v_{C1} (Equation (25)) [41].

$$\begin{cases} \frac{di_L}{dt} = -\frac{1}{L}v_{C1} + \frac{\lambda}{L}v_{DC} \\ \frac{dv_{C1}}{dt} = \frac{1}{C1}i_L - \frac{1}{C1}i_o \end{cases} \tag{25}$$

where L is the converter inductor, C_1 is the output converter capacitor in Buck mode, v_{C1} is voltage over of the output converter capacitor, i_L is the inductor current, i_o is the output current, and v_{DC} is the converter input voltage.

Considering v_{C1} as the desired controlled output voltage, it is possible to rearrange Equation (25) considering the canonical controllability form, which is expressed by Equations (26) and (27). Notice that the output current i_o in Figure 4b is equivalent to the

output current I_{PV} of Figure 5, and v_{C1} in Figure 4b is equivalent to V_{PV} in Figure 5, where ϕ is the voltage derivative over the time of the capacitor C1 [41].

$$\frac{d}{dt} \begin{bmatrix} v_{C1} \\ \phi \end{bmatrix} = \begin{bmatrix} \phi \\ -\frac{1}{LC1}v_{C1} - \frac{1}{C1}\frac{di_o}{dt} + \frac{\lambda}{LC1}v_{DC} \end{bmatrix} \tag{26}$$

$$\phi = \frac{i_L - i_o}{C1} \tag{27}$$

From the state-space equation presented in (26), it is possible to realize that i_o has a strong relative degree of two [37] (which means that the controllable variable is obtained by the second time derivative). Thus, in this condition, the sliding surface specified in (28) is sufficient to ensure the necessary stability and robustness of the closed-loop control system as given by [38]. Parameter β defined in (28) is associated with the time constant of the first-order response of the input current ($\beta > 0$). Based on (26) and (28), it is now possible to define a theoretical sliding surface as described by Equation (29).

$$S(e_{v_{C1}}, e_{\phi}) = (v_{C1ref} - v_{C1}) + \beta(\phi_{ref} - \phi) \tag{28}$$

$$S(e_{v_{C1}}, e_{\phi}) = (v_{C1ref} - v_{C1}) + \beta \frac{dv_{C1ref}}{dt} - \frac{\beta}{C1}(i_L - i_o) \tag{29}$$

However, in terms of the DC–DC power converter, it is necessary to impose a limited bandwidth on the gate drive due to the limited switching frequency of power transistors. In practical applications, this is usually undertaken using a hysteresis comparator which maintains the sliding surface near zero with a restricted switching frequency. Finally, the control law for transistor T_1 is given by Equation (30), where Δ introduces restrictions to the switching frequency.

$$\begin{cases} \text{if } S(e_{v_C}, e_{\theta}) > \Delta \text{ or } \left[\dot{S}(e_{v_C}, e_{\theta}) < 0 \text{ and } |S(e_{v_C}, e_{\theta})| < \Delta \right] \text{ then } T_1 \rightarrow \text{Turns On;} \\ \text{if } S(e_{v_C}, e_{\theta}) < -\Delta \text{ or } \left[\dot{S}(e_{v_C}, e_{\theta}) > 0 \text{ and } |S(e_{v_C}, e_{\theta})| < \Delta \right] \text{ then } T_1 \rightarrow \text{Turns Off;} \end{cases} \tag{30}$$

5. Simulation Results

To simulate the operation of the proposed system, MATLAB/Simulink software was used. Regarding the buck–boost DC–DC converter to simulate the SPV panel, the model presented in Section 3 combined with the sliding mode control strategy described in Section 4 was selected. The parameters for this model were obtained from the ASE-100-GT-FT Schot Solar Panel datasheet available online [42]. It is also possible to obtain parameters from several SPV panels using the PVsyst software database [43], as presented in the screenshot example of Figure 6.

According to the data available, (see Figure 7) the I - V and P - V characteristic curves for different irradiation values and operating temperatures were previously plotted. These results are only used for the purpose of testing the equations and parameters of the chosen SPV. Such simulation results are useful to compare with the experimental results presented in the next section.

The first simulation tests were created in test panel mode (mode I) to obtain different characteristic curves of the chosen SPV panel and evaluate the voltage and current variation. The selected components for the DC–DC converters used in the simulations are described in Table 3.

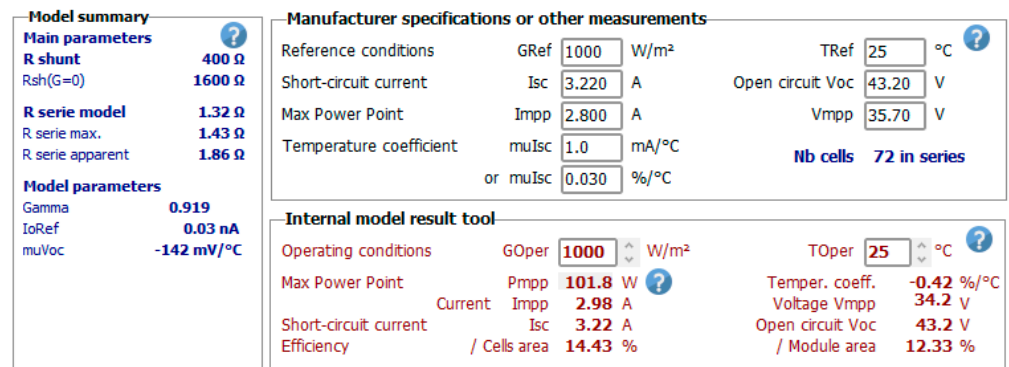


Figure 6. Example of parameters available in the PVsyst software database [43] obtained online. Model ASE-100-GT-FT.

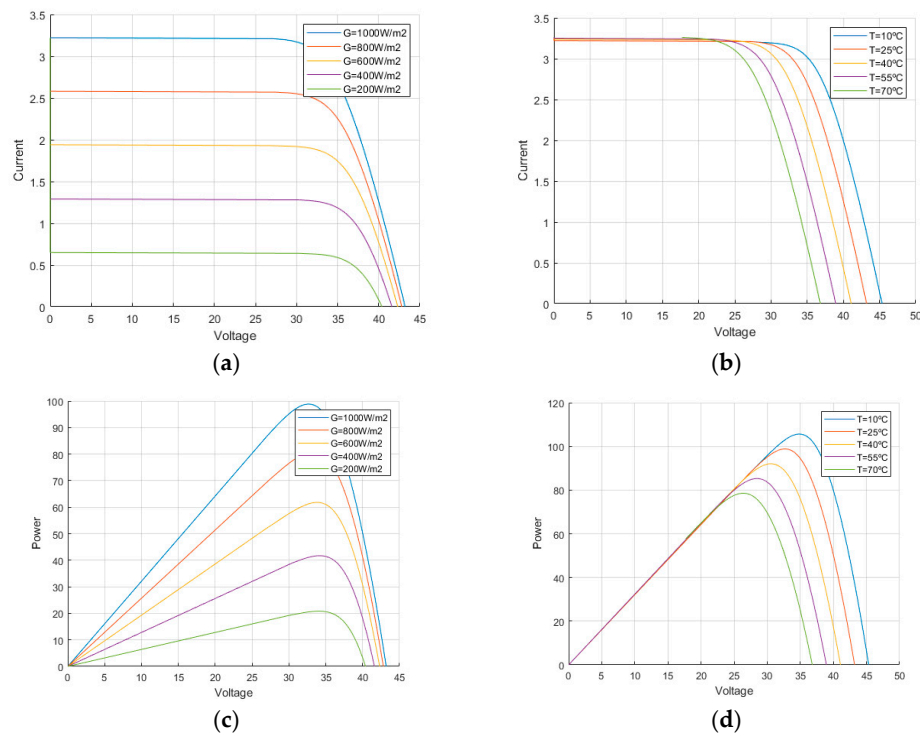


Figure 7. Simulation results of the characteristic curves for SPV model ASE-100-GT-FT considering different irradiances and operating temperatures: (a,b) I-V characteristic; (c,d) P-V characteristic.

According to the proposed control of the SPV panel simulator presented in Section 4, a simulation test to evaluate the performance of the proposed simulator was developed. Figure 8 shows the simulation diagram, based on Equation (23), in MATLAB/Simulink of the proposed SPV simulator using the buck converter.

Figure 9 presents the result of a simulation test where a continuous load variation was performed to obtain the voltage variation at the terminals of the DC–DC converter. In Figure 9a, it is possible to see the continuous current variation, and Figure 9b shows the voltage variation considering fixed values of $G = 1000 \text{ W/m}^2$ and $T_S = 25 \text{ }^\circ\text{C}$. Figure 9c shows the simulation test of the voltage variation considering that initially $G = 600 \text{ W/m}^2$, and at $t = 0.5 \text{ s}$, a step to $G = 1000 \text{ W/m}^2$ was produced. Notice that in this last simulation test, the system increases the voltage after $t = 0.5 \text{ s}$ and drops again with the increase in the current load, similar to Figure 9b. This shows that the output voltage increases with solar irradiation and decreases when the load increases, as expected.

Table 3. Components selected for the DC–DC converters used in the simulations.

Parameter	Value
Inductors	$L = 1 \text{ mH}$
Capacitors	$C1 = C2 = 470 \text{ }\mu\text{F}$
Input Voltage (first converter)	$V_{DC} = 60 \text{ V}$
Voltage at MPP	34.2 V
Current at MPP	2.98 A
Power at MPP	10.8 W
Open-circuit voltage	42.2 V
Short-circuit current	3.22 A
Equivalent shunt resistor	$400 \text{ }\Omega$
Equivalent series resistor	$1.32 \text{ }\Omega$
Power switches	$R_{on} = 10^{-3}$
Diodes	$R_{on} = 10^{-3} \text{ }\Omega$; $V_f = 0.8 \text{ V}$
Load (last converter)	$R = 100 \text{ }\Omega$; $L = 0.5 \text{ mH}$;

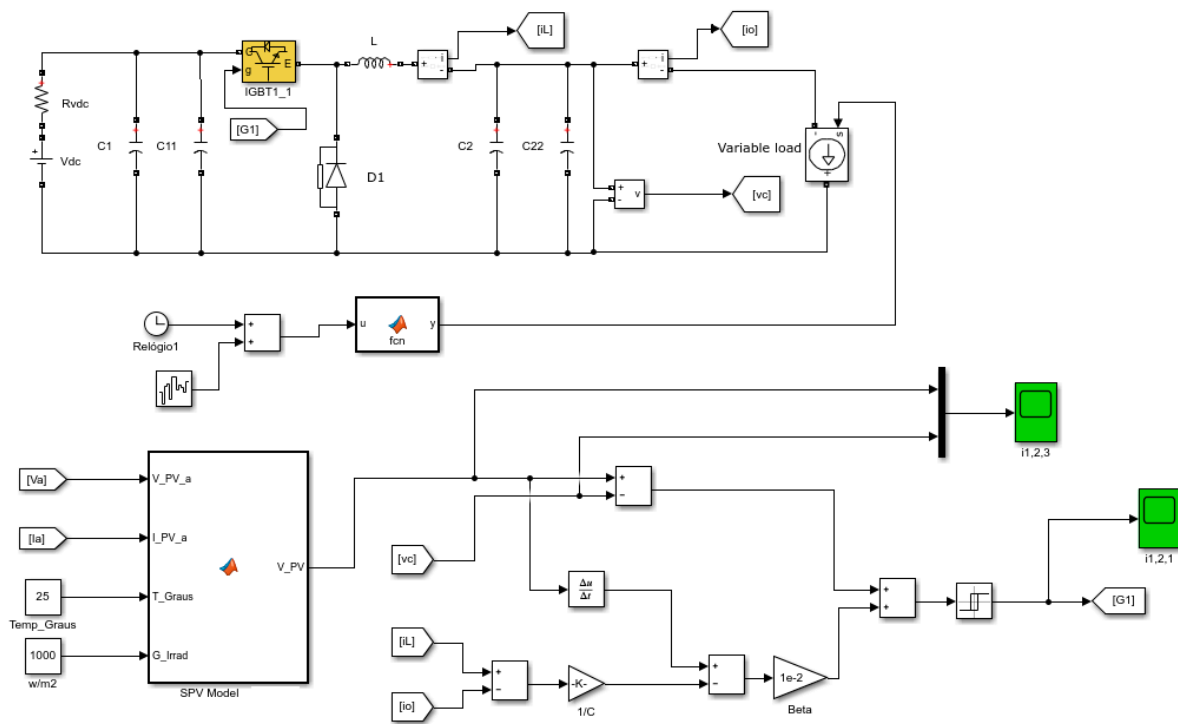


Figure 8. Matlab/Simulink model of the proposed SPV simulator using the buck converter to simulate mode I.

Some simulation tests were also performed in *MPPT* test mode (mode II) to evaluate the dynamic response of the *MPPT* algorithm chosen (in this case, the *P&O*). Similarly, the parameters are those proposed in Table 3. Figure 10 shows the simulation diagram in MATLAB/Simulink to simulate mode II.

The simulation result of this test is shown in Figure 11. Based on this result, it is possible to observe that, despite the attempt to perform a load variation at 0.25 s, then at 0.5 s, and finally, at 0.75 s, the proposed solution always supplies the load with approximately 100 W due to the *MPPT* algorithm running in the PLC and consequent PWM signal applied to the DC–DC converter. Notice that the simulation waveforms shown in this figure correspond to the output values of the converter operating in Boost mode.

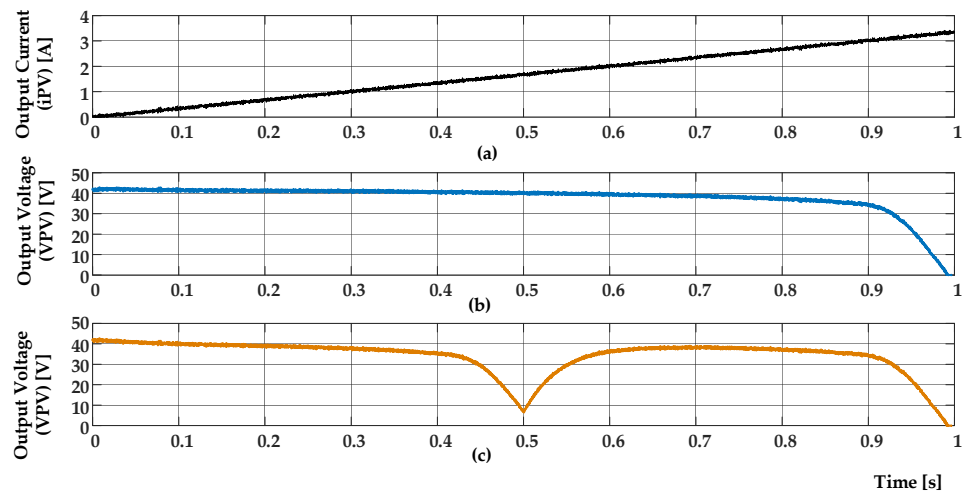


Figure 9. Simulation results considering the system operating in mode I (test panel mode): (a) continuous load variation with output current increasing; (b) output voltage variation with load variation considering a fixed $G = 1000 \text{ W/m}^2$ and $T_s = 25 \text{ }^\circ\text{C}$; (c) output voltage variation with load variation initial with $G = 600 \text{ W/m}^2$ and step to $G = 1000 \text{ W/m}^2$ at $t = 0.5 \text{ s}$.

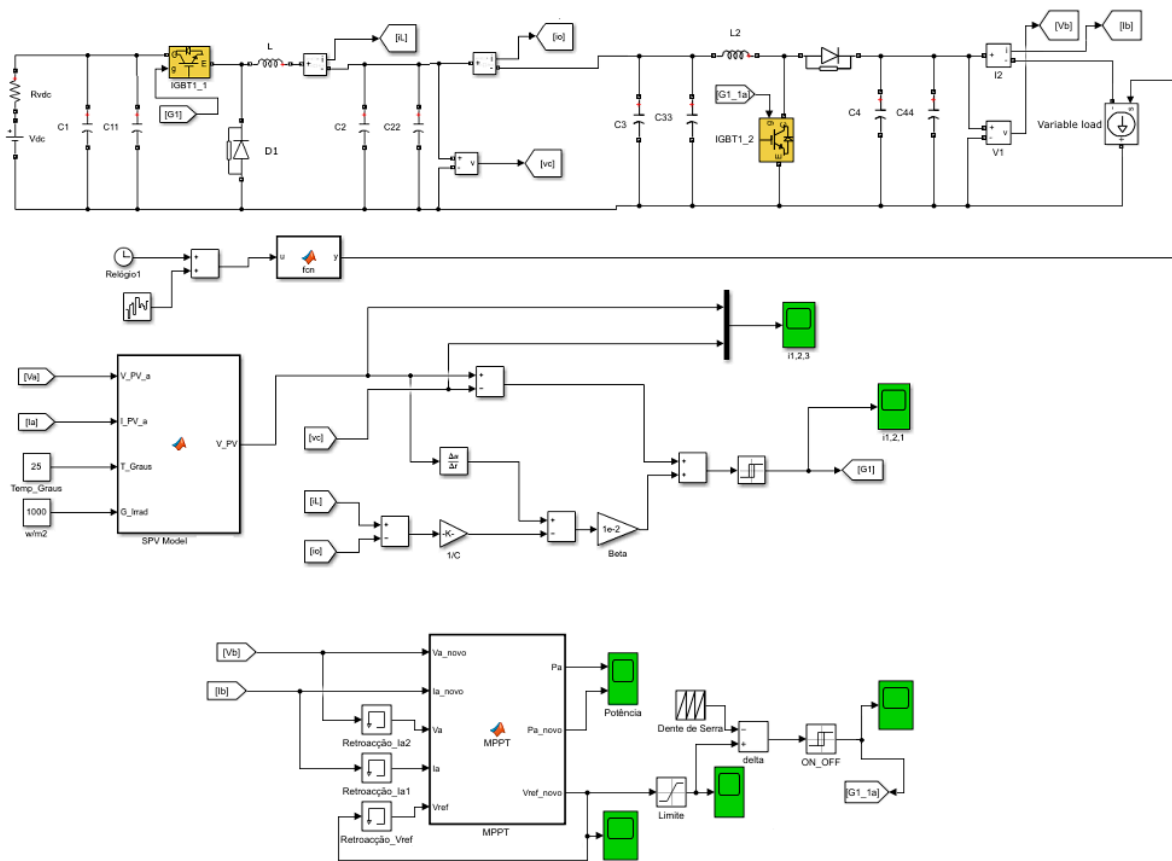


Figure 10. Matlab/Simulink model of the proposed simulator to test mode II.

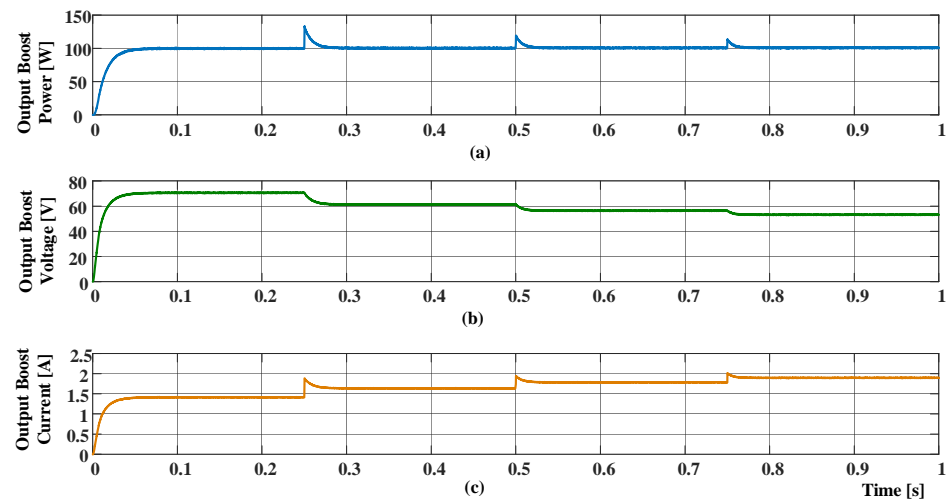


Figure 11. Simulation results considering the system operating in mode II (*MPPT* test mode): (a) output power, (b) output voltage, and (c) output current of the boost converter controlled using the perturb and observe (*P&O*) *MPPT* algorithm.

6. Experimental Results

This section is dedicated to presenting some experimental results that were obtained using a laboratorial prototype of the proposed *SPV* simulator. Some details of this prototype can be seen in Figure 12. Figure 12a shows a general overview of the prototype, where it is possible to see three buck–boost *DC–DC* converters; each green *PCB* (printed circuit board) includes two power devices (C2M0080120D SiC MOSFET) and respective drive circuits, three inductors, a red *PCB* with current sensors, a yellow *PCB* with voltage sensors, a *PLC* AXC1050-PN (Phoenix Contact), and a Microchip *DSP* microcontroller 30F4012. To supply the system, a laboratorial *DC* power supply adjusted to 60VDC was used. The values of the passive components of the *DC–DC* converters are $C_1 = C_2 = 470 \mu\text{F}$, $L = 1 \text{ mH}$. Figure 12b shows in detail the *DC–DC* power converter and the inductor adopted.

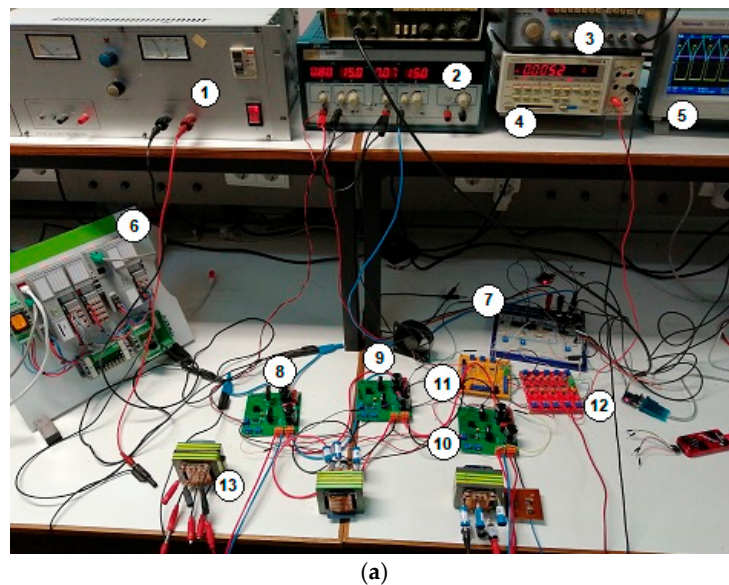
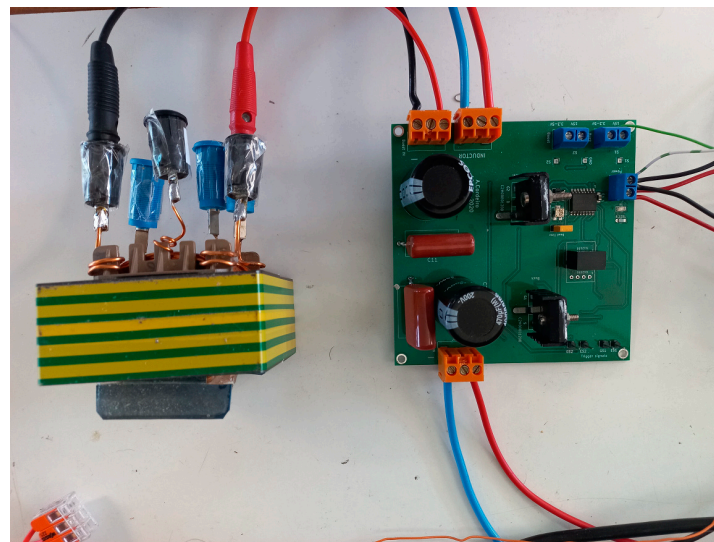


Figure 12. Cont.



(b)

Figure 12. Experimental setup of the proposed system; (a) general overview of the prototype, 1—DC power source, 2—power source to supply control circuit, 3—signal generator, 4—multimeter, 5—oscilloscope, 6—PLC AXC1050 controller from Phoenix Contact, 7—microchip DSP microcontroller 30F4012, 8—first DC–DC converter, 9—second DC–DC converter, 10—third DC–DC converter; 11—voltage sensor PCB, 12—current sensor PCB, 13—inductors; (b) detail of the DC–DC power converter and inductor adopted.

The components and circuits used in the laboratory prototype to perform the experimental tests are described in Table 4.

Table 4. Components and circuits used in the laboratory prototype.

Component or Circuit	Value
Inductors	$L = 1 \text{ mH}$ (manually created)
Capacitors	EPCOS–C1 = C2 = 470 μF , 200 V
Power Devices	C2M0080120D SiC MOSFET (1200 V; 36 A) with freewheel diode
Filtering capacitors	2.2 μF , 400 V
Isolated drive circuits	TI–UCC21520DW
Auxiliary Isolated power sources	Murata–NMA1215SC
Main Power Source	Wanptek–100VDC; 20 A.
DSP device	Microchip DSPIC30F4012
DAC device	Microchip 12-bits MCP4922
PLC	Phoenix Contact–ACX-1050-PN
Current sensors	ACHS7122; Current range: $\pm 20\text{A}$; Sensitivity: 100 mV/A; Primary conductor resistance: 0.7 m Ω ; Bandwidth: 80 kHz; Total output error of $\pm 1.5\%$
Voltage sensors	AMC1100; $\pm 250 \text{ mV}$ input voltage range optimized for shunt resistors; Offset error: 1.5 mV; Input bandwidth: 60 kHz min; Fixed gain: 8 (0.5% Accuracy).

The following figure presents the diagram of the proposed buck–boost DC–DC converter on the PCB (printed circuit board) design using the Kicad software (see Figure 13a) and the respective isolated drive circuit using the UCC21520DW chip (see Figure 13b). In the proposed project, the current and voltage sensors were not introduced in the PCB of

the DC–DC circuit. These devices are placed in other multipurpose boards to be applied in different projects whenever necessary. Figure 13c shows the red PCB with five current sensors (ACHS7122) with multiple adjustments (gains and offsets) and the yellow PCB with three voltage sensors (AMC1100) also with multiple adjustments (gains and offsets).

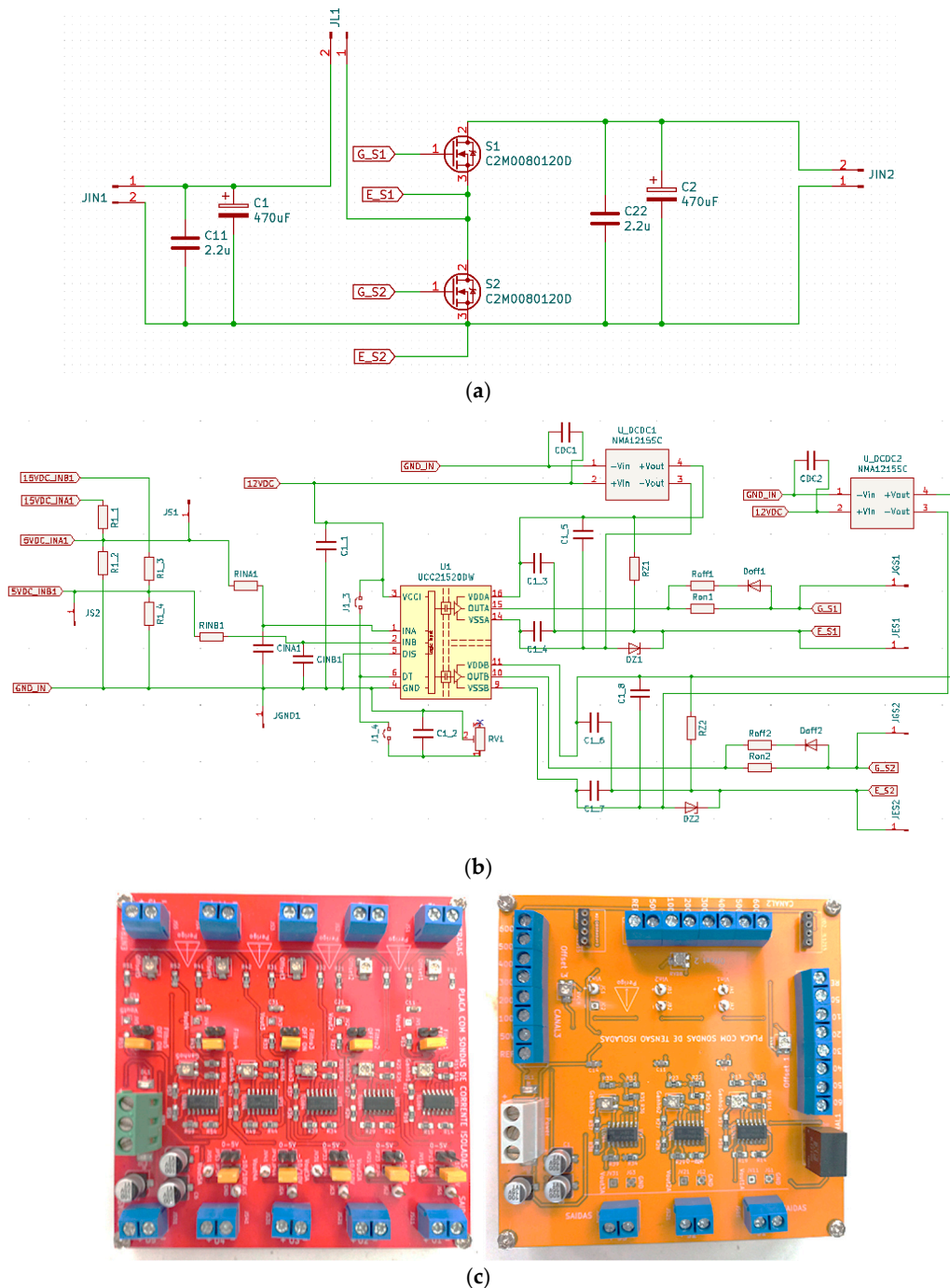


Figure 13. (a) Diagram of the proposed buck–boost DC–DC converter on the PCB (printed circuit board) design using the *Kicad* software; (b) Isolated drive circuit using the UCC21520DW chip placed in the DC–DC board; (c) Photographs of the PCBs with current sensors (five ACHS7122), red PCB and voltage sensors (three AMC1100), yellow PCB.

The first experimental tests were carried out to evaluate the operation of the buck–boost DC–DC power converter associated with the *SPV* simulator and the *DSP* microcontroller to accomplish the current–voltage characteristic curves (mode I). Those results can

be seen in Figure 14. Figure 14a shows the output voltage (Ch1–7.5 V/div) and output current (Ch2–0.6 A/div) of the buck–boost DC–DC converter considering a continuous load variation. As this automatic test takes some time to complete using step load variations, it was connected to a multi-turn variable load available in the laboratory to perform a quick test to record the waveforms with the oscilloscope. The operator manually turns several resistors in parallel to perform the load variation. In this figure, it is possible to see the voltage variation as the current increases considering the parameters introduced by the operator (see Figure 14a), $G = 1000 \text{ W/m}^2$ at $T = 25 \text{ }^\circ\text{C}$. Figure 14b shows a similar result considering a continuous load variation and a solar irradiation step from $G = 600 \text{ W/m}^2$ to $G = 1000 \text{ W/m}^2$ at $T = 25 \text{ }^\circ\text{C}$. To conclude about the current–voltage characteristic curves and their proximity to real operation, the developed SCADA software records several data points from each test. Figure 14c,d shows the average data points of the I - V and P - V characteristic curves achieved during a practical test considering $G = 1000 \text{ W/m}^2$ at $T = 25 \text{ }^\circ\text{C}$. These results exhibit similar characteristics curves indicating a good approximation of the SPV panel model (one diode model), parameters, and dynamics of the DSP microcontroller. The experimental results revealed that, above a certain current value, it becomes difficult to obtain valid voltage readings due to excessive ripple in the DC–DC converters.

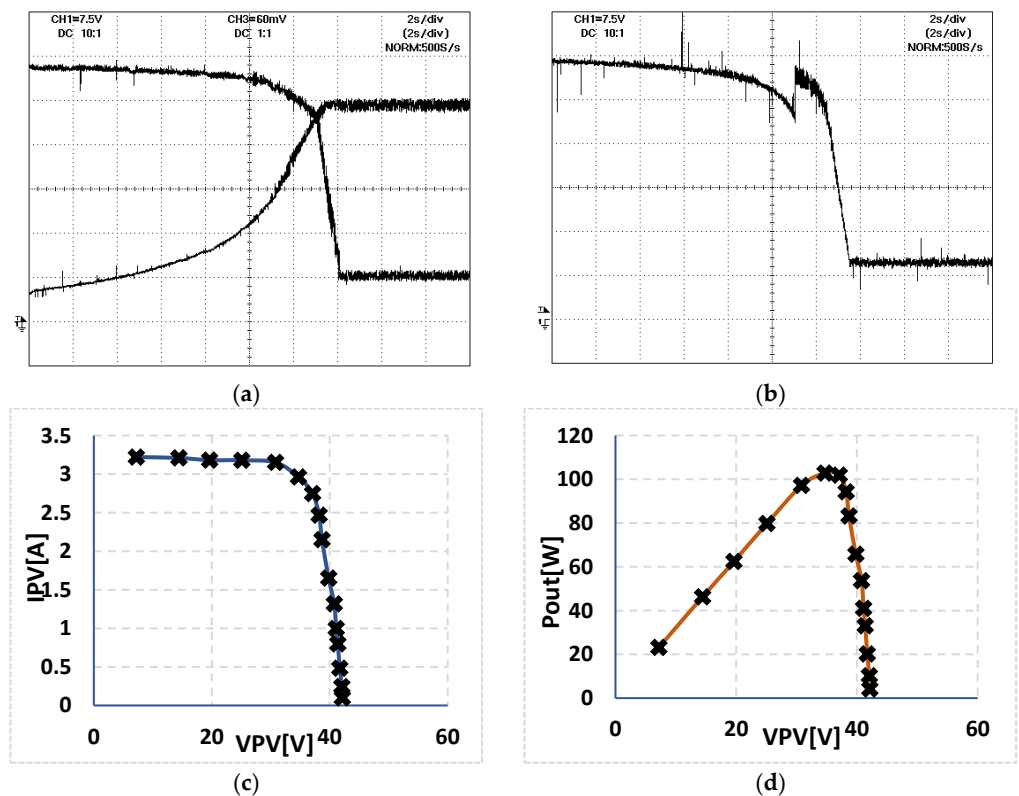


Figure 14. Experimental result in test panel mode (mode I): (a) output voltage (Ch1–7.5 V/div) and output current (Ch3–0.6 A/div) during a continuous load variation; (b) Similar to (a) considering a step solar irradiation from $G = 600 \text{ W/m}^2$ to $G = 1000 \text{ W/m}^2$ both at $T = 25 \text{ }^\circ\text{C}$; (c) average data points recorded by the SCADA software for the I - V characteristic curves, at $G = 1000 \text{ W/m}^2$ and $T = 25 \text{ }^\circ\text{C}$; (d) Similar to (c) applied to P - V characteristic curves.

Additional experimental tests were performed to evaluate the performance of the system in mode II (MPPT test mode). Two experimental results in this scenario can be seen in Figure 15. The $P\&O$ MPPT algorithm was selected and designed to continuously control the duty cycle of the buck–boost DC–DC power converter. Figure 15a presents the output power (Ch3), output voltage (Ch1–50/div), and output current (Ch2–1A/div) of the buck–boost converter. Observing Figure 15, it is possible to conclude that the solution is

able to generate the same output power for different weather conditions with an acceptable response. Despite the attempt to perform a load variation, when the user attempts to increase the load, the MPPT controller reduces the output voltage, which maintains the same output power. Figure 15b shows several data points achieved during the operation of the MPPT algorithm. Observing this figure, it is also possible to see that the MPPT is able to maintain the MPP (*maximum power point*) around the expected value despite some dispersion and a moderate response time.

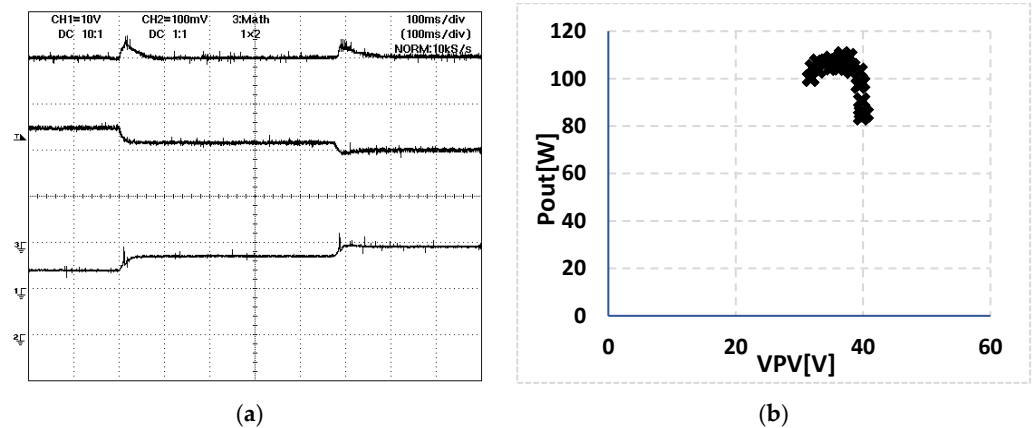


Figure 15. Experimental result in mode II (MPPT test mode): (a) output power (Ch3), output voltage (Ch1–50/div) and output current (Ch2–1A/div) of the boost converter considering two-step load variations; (b) multiple data points achieved during the operation of the P&O MPPT algorithm.

The next figure shows the layout of the SCADA software developed to introduce the parameters of the SPV panel, temperature, and irradiation. These values are then sent to the PLC, which retains all data and sends them to the DSP microcontroller. The SCADA layout was developed in the VISU+ software from Phoenix Contact, and the same manufacturer of the PLC was adopted. The software operates in real time, and the data exchange is updated each 500 ms, the minimum value allowed by the software, in the available version. In the basic version, this software has three communication drives available (PROFINET, Modbus TCP/IP, and INTERBUS). The Modbus TCP/IP communication drive was selected to communicate with the PLC. The Modbus TCP/IP was preferred over the well-known PROFINET since this allows the SCADA solution to operate in controller (master) mode, whereas PROFINET was only available in device (slave) mode. The PLC adopted is the model AXC1050 PN from Phoenix Contact. The description of the automated tests is described next.

The operator must choose which mode (mode I or mode II) is going to execute in the SCADA layout. When mode I is selected, the operator must connect the output of the first converter (in buck mode) to the input of the third converter (also in buck mode). Then, they must connect the fixed RL load to the output of the third converter (this could also be performed using relays to connect and disconnect the converters, but in this case, it is performed manually). Next, the operator must introduce in the SCADA software all the desired parameters from the PV panel and also irradiance and temperature. The operator must define up to 15 desired load variations in the SCADA software. After these procedures, the operator starts the automated test in the SCADA software. The SCADA software sends all the information to the AXC1050 PN PLC over the Modbus TCP/IP protocol. After receiving the data, the PLC adjusts the duty cycle of the third converter to the first load variation step. Then, the PLC sends all the parameters to the DSP device, namely, the panel parameters, solar irradiance, and temperature. Finally, the DSP device, which has the SPV model programmed, updates the parameters and starts to read the output current and the voltage output of the first converter (buck converter as an SPV simulator) and, according to the model equations, updates the voltage reference of the converter which,

using the control strategy, adjusts the duty cycle of the power switch of the converter. The PLC also records the output current and voltage of the first converter every second and sends these values to the SCADA program to show them in a trend chart. After a defined number of running cycles, the PLC adjusts the second load step, and all these procedures are repeated until the end of load variations. During this process, the parameters of the SPV panel, solar irradiance, and temperature cannot be changed until the end of the automated test. Nevertheless, the operator can stop the ongoing test at any moment, updating the values, and can restart a new automated test again. The SCADA system records the result of all the automated tests in the .csv format to be used in Excel. The following flowchart, presented in Figure 16, describes the automated test procedure applied to mode I.

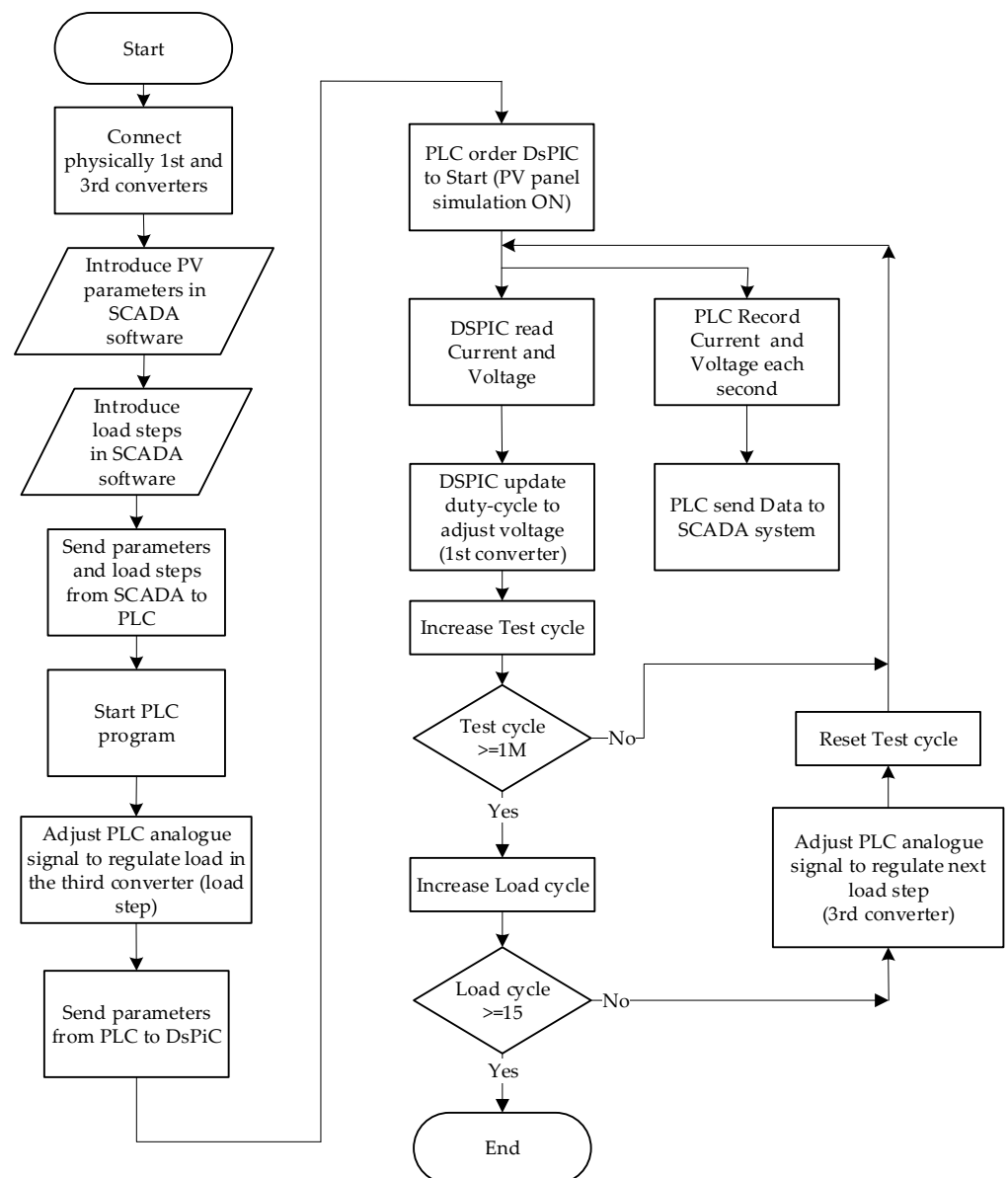


Figure 16. Flowchart of the automated test procedure applied to mode I.

In the case of selecting mode II, the operator must connect the output of the first converter (in buck mode) to the input of the second converter (in boost mode). Then, the output of the second converter must be connected to the input of the third converter (buck converter). Then, a fixed RL load must be connected to the output of the third converter. To summarize, all the converters must be connected in series. The main difference is such that, the operator must now select mode II and the desired MPPT algorithm in

the SCADA software. The following procedures are similar to mode I, but in this case, besides the adjustment of the load step, the PLC also regulates the duty cycle (through the analogue output connected to a PWM modulator) of the second converter to achieve the MPP continuously. Notice that the DSP device is only running the SPV model, reading the current and voltage, and updating the voltage reference. This is critical to avoid delays in the process. The non-critical speed actions are performed by the PLC. The flowchart presented in Figure 17 describes this procedure to mode II.

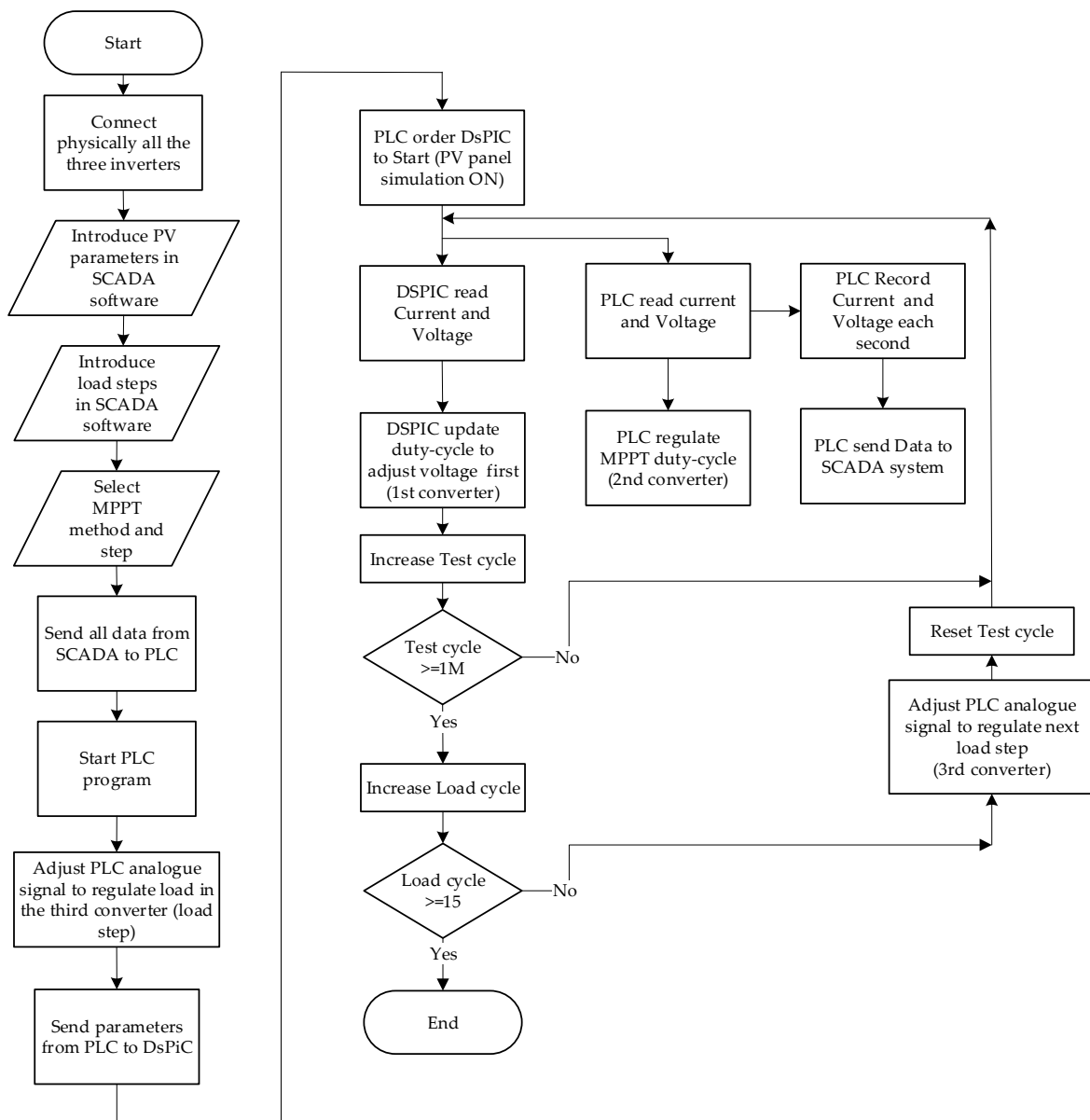


Figure 17. Flowchart of the automated test procedure applied to mode II.

The DSP device is programmed to run the SPV model, read the current and voltage, and update the output voltage reference. The SPV model requires the readings of previous output currents and voltage step cycles, and the result of the model equation gives the voltage reference to a DAC device, which is used as an output voltage reference to the sliding mode control loop. The DSP device is also used to communicate with the PLC, mainly receiving information to update the parameters and operation conditions. Notice that the output current and voltage of the first converter are used by the DSP device, and

they are not sent by RS-232-C communication to the PLC. The PLC has individual analogue variables dedicated to reading this output current and voltage to speed up the process.

A simplified pseudocode of the PLC, DSPIC, and SCADA program can be found in Figures 18–21, respectively.

```

Run_Task ()
{
  If NewUpdateMsgReceived() Then %message send from PLC via ModbusTCP
  {
    UpdateData(); %Update data in the PLC memory registers
    SendDataRS232C(); % Send Data to DSPIC 30F4012
  }
  Endif
  If NewStartMsgReceived() Then %Msg from SCADA given order to start
  {
    xStartBit := True; %Enable Start Bit
    iDataReceived.LoadStep := 1; %Start in the first load step
    SetAnalogueOutput(DataReceived.LoadStep); % Adjust Step Analog Ouput
    SendStartRS232C(); % Send Start Bit to DSPIC 30F4012
    If DataReceived.Mode2() Then %Mode2 was activated in SCADA
      xMode2Bit := True; %Enable Mode 2
    Endif
  }
  Endif
  If xStartBit Then
    For Each DataReceived.TotalLoadSteps %Repeat for all the Load Steps
    {
      Timer1.Restart :=True; Timer1.Start :=True; %Restart Timer1
      Repeat Until Timer1.Value < 20000ms %Repeat test for 20 seconds
      {
        Vn := Measure_Analogue_Ch1(); %Measure last Voltage value in Ch1
        In := Measure_Analogue_Ch2 (); %Measure last Current value in Ch 2
        %SCADA request data?
        If SCADARequestData() Then
          SendMeasurements(); %Send Voltage and current to SCADA
        Endif
        %Mode 2 activated?
        If xMode2Bit Then
          {
            If DataReceived.MPPT=1 Then
              Call Procedure_MPPT_P&O(); %Call the Perturb and Observe MPPT
            Elseif DataReceived.MPPT=2 Then
              Call Procedure_MPPT_INC_CON(); %Call the Increm. Conduct. MPPT
            Else
              Call ....%Other MPPT Algorithms
            Endif
          }
        Endif
      }
    }
    iDataReceived.LoadStep := iDataReceived.LoadStep +1; %Next Load Step
    SetAnalogueOutput(DataReceived.LoadStep); % Adjust Step Analog Ouput
  End For
  xStartBit :=False; %Disable Start Bit
Else
  SendStopRS232C(); % Send Stop Bit to DSPIC 30F4012
Endif
}
End_Run_Task()

```

Figure 18. Simplified pseudocode of the main PLC task (developed in Structured Test according to IEC61131-3).

```

Procedure_MPPT_P&O()

C := 0.01; Step value
Vn := Measure_Analogue_Ch1(); %Measure last analogue value in Channel 1
In := Measure_Analogue_Ch2 (); %Measure last analogue value in Channel 2
Pn := Vn x In; % Calculate Power
DeltaP := Pn-(Pn-1); %Power difference with last one
DeltaV := Vn-(Vn-1); %Voltage difference with last one
%-----P&O Algorithm
If (DeltaP > 0.0) and (DeltaV > 0.0) Then
    Vref := Vref + C;
ElseIf (DeltaP > 0.0) and (DeltaV < 0.0) Then
    Vref := Vref - C;
ElseIf (DeltaP < 0.0) and (DeltaV > 0.0) Then
    Vref := Vref - C;
ElseIf (DeltaP < 0.0) and (DeltaV < 0.0) Then
    Vref := Vref + C;
Endif
%-----
%At maximum value
If (DeltaP = 0.0) Then
    Vref := Vref;
Endif
%Maximum analogue Output Limit
If (Vref > 10.0) Then
    Vref := 10.0;
Endif
%Minimum analogue Output Limit
If (Vref < 0.0) Then
    Vref := 0.0;
Endif
End_Procedure_MPPT_P&O ()

```

Figure 19. Simplified pseudocode of the perturb and observe MPPT algorithm running in the PLC (developed in Structured Test-IEC61131-3).

The main variables and configuration statements of the DSP device are indicated in Tables 5 and 6.

Figure 22 shows the layout of the SCADA software developed to introduce the parameters of the SPV, solar irradiance, and temperature.

Figure 23 shows the layout of the SCADA software developed to present and record data (voltage, current, power) obtained by the PLC during experimental tests, selecting the MPPT algorithm, load step variation, and other information.

```

%Configuration and declaration section
#pragma config statements (see table 5);
#include <xc.h>; #include <p30F4012.h>; #include <math.h>; #include <uart.h>; #include <stdlib.h>;
#include "comm.h"; #include "analog.h"; #include "timer.h";
Variable Declaration (see table 6)
%Main program
int main(void) {
    %Initialize peripheral
    Uart1_start(); Uart2_start(); Timer1_start(); ADC_start(); SPI_Start(); PutsUART1("Startup ok\r\n");
    %Initialize Variables before communication
    VPVref = 0; T = 25; G = 1000; VOC_STC = 43.2; ISC_STC = 3.22; RS = 1.86; RT=400; Ki = 0.001;
    Kv = -0.142; n = 0.919; Ncell = 72;
    %Main Loop
    While (1)
    {
        If ReceivedDataRS232C() Then
            UpdateVariables(); %Update declared variables from the SCADA over the PLC
        Endif
        If ReceivedStartRS232C() Then %Message to Start Calculations
        {
            VPV=ADC_read(0)*(60.0/1023.0); %Read Voltage Analogue
            IPV=ADC_read(1)*(5.0/1023.0); %Read Current Analogue
            %Perform calculation in sections
            dT = T - 25;
            VT = 0.000086173*(T+273.15)*Ncell;
            IO = (dT*Ki + ISC_STC)/(exp((VOC_STC + Kv*dT)/(n*VT))-1);
            VOC = ((VOC_STC + (dT * Kv))*(G/1000));
            ISC = ((ISC_STC + (dT * Ki))*(G/1000));
            % Avoid Negative values due to noise
            If (IPV>ISC) Then
                IPV=ISC-0.01;
            Endif
            VPVref = n*VT*log((ISC-IPV+IO)/IO)-RS*IPV; %Result in real values
            VPVref5V = VPVref*(5.0/60.0); %Result updated to Analog Output of 5V
            VPVrefWord = (int)(VPVref/0.0146484375); %Converter to integer
            SPI_Write(VPVrefWord); %Send to DAC over SPI protocol
            %Show calculation results and variables in the PC screen to monitoring
            PutsUART1("Variables:\r\n");
            PutsUART1(rxbuffer2);
            T=atof(rxbuffer2+3); G=atof(rxbuffer2+10); VOC_STC=atof(rxbuffer2+17);
            ISC_STC=atof(rxbuffer2+24); RS=atof(rxbuffer2+31); RS=atof(rxbuffer2+22);
            Kv=atof(rxbuffer2+38); Ki=atof(rxbuffer2+45); n=atof(rxbuffer2+52);
            Ncell=atof(rxbuffer2+59);
            sprintf(buffer, "PA%6.2f#%6.0f#%6.2f#%6.2f#%6.2f#%6.3f#%6.3f#%6.0f#", T, G,
                VOC_STC, ISC_STC, RS, Kv, Ki, n, Ncell);
            putsUART2(buffer);
        }
    }
    Endif
}
Loop()

```

Figure 20. Simplified pseudocode of the DSP device programmed in C code.

Comparison aspects between several *SPV* simulators proposed in the literature are presented in Table 7. This comparison takes into account the following aspects: solution novelty regarding the *SPV* model; the accuracy of the proposed simulator regarding theoretical equations; the model supported by simulations and/or experimental results; the proposed solution explores a new or any *MPPT* algorithm; the complexity of the proposed simulator; the ability to perform and record the automated tests; the existence of any *SCADA* or *HMI* (human–machine interface), and the estimated hardware cost when available.

```

%Routine of SCADA Main window in Visu+ software
Declaration of Variables here;
SCADA_Main ()
{
  If SendButtonPressed() Then %if send button pressed
  {
    If ProcessStoped() Then %The process is Stoped?
    {
      If DataValuesOnRange() Then %Data is on the desired range?
      {
        If LoadStepsSelected() Then %Load steps were introduced?
        {
          SendDataToPLC(); %message send to PLC via ModbusTCP
          TimerComm.Restart :=True; TimerComm.Start :=True; %Restart TimerComm
          Delay 2 seconds; %This give time to PLC send data to DSP device
          Call OpenChartWindow(); %Open the window to show received data
          SendStartMsgToPLC();
        }
        Else
          MsgBox ("Load step not defined or missing values")
        Endif
      Else
        MsgBox ("Data Range is invalid or missing values")
      Endif
    }
    Else
      MsgBox ("Process is running. Not possible to send data")
    Endif
  }
Endif
If UpdateDataButtonPressed() Then %if Update button pressed
  Call UpdateDataWindow(); %Open the window to introduce parameters
  Call UpdateLoadStepWindow(); %Open the window to introduce load steps
Endif
If ProcessRunning() Then %If the process is running?
  {
    If TimerComm.Value < 1000ms
      Do nothing;
    Else %Request Voltage and Current values at each second
    {
      RequestPLCMeasurements(); UpdateMemoryMeasurements(); RecordDataCsv();
      TimerComm.Restart :=True; TimerComm.Start :=True; %Restart TimerComm
    }
  Endif
}
Endif
If StopButtonPressed() Then %if Update button pressed
  UpdateProcessState();
  SendStopMsgToPLC(); %Order to Stop the PLC and DSP device
Endif
}
End SCADA_Main ()

```

Figure 21. Simplified pseudocode of the main window of SCADA software in C code.

Table 5. Configuration statements of the DSP device.

Configuration Statements	Value
%Oscillator	
#pragma config FPR	FRC_PLL16 %Primary Oscillator Mode (FRC
#pragma config FOS	PRI %Oscillator Source (Primary Oscillator)
#pragma config FCKSMEN	CSW_FSCM_OFF %Clock Switching and Monitor
%Watchdog	
#pragma config FWPSB	WDTPSB_16 %WDT Prescaler B (1:16)
#pragma config FWPSA	WDTPSA_512 %WDT Prescaler A (1:512)
#pragma config WDT	WDT_OFF %Watchdog Timer (Disabled)
%Voltage Protection	
#pragma config FPWRT	PWRT_64 %POR Timer Value (64 ms)
#pragma config BODENV	BORV42 %Brown Out Voltage (4.2 V)
#pragma config BOREN	PBOR_ON %PBOR Enable (Enabled)
#pragma config MCLR	MCLR_EN % Master Clear Enable (Enabled)
%Code protection	
#pragma config GWRP	GWRP_OFF %General Code Segment Write Protect
#pragma config GCP	CODE_PROT_OFF %General Segment Code Protection
%Programming	
#pragma config ICS	ICS_PGD %Comm Channel Select (Use PGC/EMUC)

Table 6. Declaration Variables of the DSP device.

Type	Variable
float	VT
float	n
float	VOC_STC
float	ISC_STC
float	IO
float	RS
float	RT
float	VOC
float	ISC
float	Ki
float	Kv
float	dT
float	T
float	G
float	Ncell
float	VPVref
float	VPV
float	VPVref5V
float	IPV
integer	VPVrefWord
integer	DataReceived = 0
char	buffer (80)
char	rxbuffer (80)
char	rxbuffer2 (80)

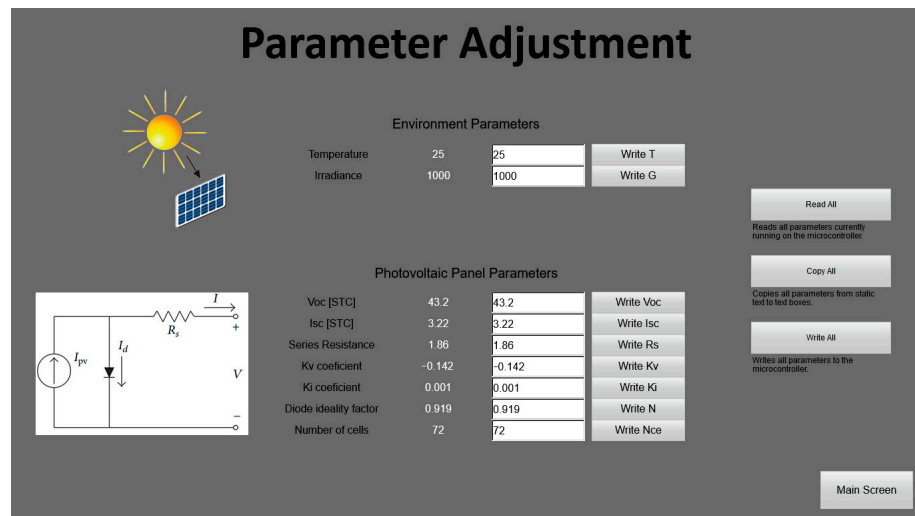


Figure 22. SCADA software layout developed to introduce parameters of the SPV panel, including temperature and irradiation.

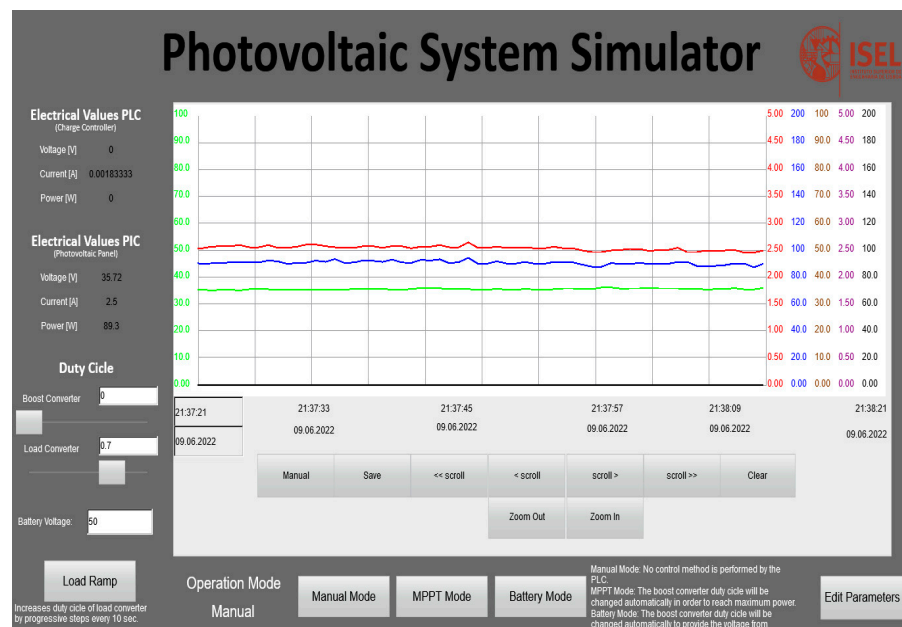


Figure 23. SCADA software layout developed to present and record data (voltage (green line), current (red line), power (blue line)) obtained by the PLC during experimental tests.

Table 7. Comparison between *SPV* simulators proposed in the literature.

Characteristics	Solution												Proposed
	[11]	[12]	[14]	[15]	[16]	[17]	[18]	[19]	[20]	[21]	[22]	[23]	
New <i>SPV</i> model	Yes	No	No	Yes	No								
Model Accuracy	Good	Med.	Good	Good	Low	Med.	Med.	Med.	Med.	Med.	Low	Med.	medium
Simulations results	Yes	Yes	Yes	Yes	Yes	No	No	No	Yes	Yes	Yes	Yes	Yes
Experimental results	No	Yes	Yes	No	Yes	Yes	Yes	Yes	No	Yes	Yes	Yes	Yes
Hardware developed	No	No	Yes	No	Yes	Yes	No	Yes	No	Yes	Yes	Yes	Yes
New MPPT algorithm	No	No	No	No	No	No	No	No	No	No	No	No	No
Any MPPT algorithm included	No	No	No	No	No	No	No	Yes	No	No	No	No	Yes
Complexity implementation	Med.	Low	Low	Med.	Low	Med.	Low	Low	Low	Low	Low	Low	Med.
Automated tests	No	No	Yes	No	No	No	Yes	Yes	No	No	No	No	Yes
SCADA/HMI interface	No	No	Yes	No	Yes	No	Yes	No	No	No	No	No	Yes
Hardware Cost	*NA	Low	High	*NA	Low	High	High	Low	*NA	Low	Low	Low	Low

*NA—not applicable.

7. Conclusions

This paper presented the development of an *SPV* simulator system based on three buck–boost *DC–DC* converters. The proposed solution can generate automatic tests in two different modes, namely, to simulate the current–voltage and power–voltage characteristic curves of *SPV* panels (test panel mode or mode I) and the *MPPT* mode (mode II), the parameters of which can be introduced in the *SCADA* software. The proposed solution is flexible and can be changed and restarted according to new values introduced by the operator. The experimental results presented in this work demonstrate the effectuality and the good performance of the sliding mode control strategy employed in the *DC–DC* converter which simulates the *SPV* panel considering solar irradiation, temperature, and load variation. The experimental results also revealed that the adopted *PLC* is able to run the *MPPT P&O* algorithm, generating acceptable results despite some dispersion and moderate response times. Furthermore, experimental results revealed that above the *MPP* current value, it becomes difficult to obtain valid data due to excessive ripple in the *DC–DC* converters. Thus, the best results achieved a current ripple between 2% to 5% of the desired average current in *MPP* conditions. The major limitation is the maximum power of the designed *DC–DC* converters (up to 365 W) and also the difficulty of running complex *MPPT* algorithms. It is possible to conclude that the proposed solution can produce good results and could be a useful tool for the simulation of theoretical concepts about solar photovoltaic energy and automation.

Author Contributions: Conceptualization, A.C., H.L. and V.F.P.; Methodology, A.C., V.F.P., D.F. and J.F.M.; Software, H.L. and T.G.A.; Formal analysis, A.C., M.C., F.B. and P.F.; Investigation, A.C., P.G., H.L. and V.F.P.; Resources, A.C., V.F.P. and J.F.M.; Writing—original draft, A.C.; Writing—review & editing, A.C., H.L. and V.F.P.; Visualization, M.C., P.G., F.B., P.F., D.F. and T.G.A.; Supervision, A.C. and V.F.P.; Project administration, A.C. and V.F.P.; Funding acquisition, A.C. and V.F.P. All authors have read and agreed to the published version of the manuscript.

Funding: This work was funded by Instituto Politécnico de Lisboa, reference code: IPL/2021/ATS2SPV_ISEL.

Data Availability Statement: Not applicable.

Acknowledgments: The authors acknowledge Phoenix Contact Portugal under the EDUNET Partnership for supplying automation devices to this work.

Conflicts of Interest: The authors declare no conflict of interest.

References

1. Baena-Moreno, F.M.; Rodríguez-Galán, M.; Vega, F.; Alonso-Fariñas, B.; Arenas, L.F.V.; Navarrete, B. Carbon capture and utilization technologies: A literature review and recent advances. *Energy Sources Part A Recovery Util. Environ. Eff.* **2019**, *41*, 1403–1433. [CrossRef]
2. IEA. International Energy Agency Report. Global Energy Review. 2021. Available online: <https://www.iea.org/reports/global-energy-review-2021> (accessed on 10 January 2023).
3. Renewables 2021 Global Status Report—A Comprehensive Annual Overview of the State of Renewable Energy, REN21. 2021. Available online: <https://ren21.net/gsr-2021/> (accessed on 10 January 2023).
4. Zampirolli, F.A.; Josko, J.F.M.B.; Venero, M.L.F.; Kobayashi, G.; Fraga, F.J.; Goya Savegnago, D.H.R. An experience of automated assessment in a large-scale introduction programming course. *Comput. Appl. Eng. Educ.* **2021**, *29*, 1284–1299. [CrossRef]
5. Osamnia, M.; Okada, H.; Berena, A.J.; Ueno, H.; Chunwijitra, S. A novel automated course generation system embedded in the online lecturing platform for higher education. *Comput. Appl. Eng. Educ.* **2016**, *24*, 586–598. [CrossRef]
6. Basheer, S.; Saleh Alluhaidan, A.; Mathew, R.M. A secured smart automation system for computer labs in engineering colleges using the internet of things. *Comput. Appl. Eng. Educ.* **2020**, *29*, 339–349. [CrossRef]
7. Chinnasamy, J.; Shankar Ramesh Babu, K.; Chenniappan, M.; Rathinasamy, P. A workbench for motion control experiments using programmable automation controllers in industrial automation laboratory at Kongu Engineering College. *Comput. Appl. Eng. Educ.* **2018**, *26*, 566–576. [CrossRef]
8. Gangwar, P.; Tripathi, R.P.; Singh, A.K. Solar photovoltaic tree: A review of designs, performance, applications, and challenges. *Energy Sources Part A Recovery Util. Environ. Eff.* **2021**, 1–28. [CrossRef]
9. Hishikawa, Y.; Doi, T.; Higa, M.; Yamagoe, K.; Ohshima, H.; Takenouchi, T.; Yoshita, M. Voltage-Dependent Temperature Coefficient of the I–V Curves of Crystalline Silicon Photovoltaic Modules. *IEEE J. Photovolt.* **2018**, *8*, 48–53. [CrossRef]
10. Mann, S.; Fadel, E.; Schoenholz, S.S.; Cubuk, E.D.; Johnson, S.G.; Romano, G. ∂ PV: An end-to-end differentiable solar-cell simulator. *Comput. Phys. Commun.* **2022**, *272*, 108232. [CrossRef]
11. Khalid, M.S.; Abido, M.A. A novel and accurate photovoltaic simulator based on seven-parameter model. *Electr. Power Syst. Res.* **2014**, *116*, 243–251. [CrossRef]
12. Ünlü, M.; Çamur, S. A simple Photovoltaic simulator based on a one-diode equivalent circuit model. In Proceedings of the 4th International Conference on Electrical and Electronic Engineering (ICEEE), Ankara, Turkey, 8–10 April 2017; pp. 33–36. [CrossRef]
13. Shannan, N.M.A.A.; Yahaya, N.; Singh, B. Single-diode model and two-diode model of PV modules: A comparison. In Proceedings of the IEEE International Conference on Control System, Computing and Engineering, Penang, Malaysia, 29 November–1 December 2013; pp. 210–214. [CrossRef]
14. Hosseini, H.S.M.; Keymanesh, A.A. Design and construction of photovoltaic simulator based on dual-diode model. *Sol. Energy* **2016**, *137*, 594–607. [CrossRef]
15. Singh, B.; Singla, M.K.; Nijhawan, P. Parameter estimation of four diode solar photovoltaic cell using hybrid algorithm. *Energy Sources Part A Recovery Util. Environ. Eff.* **2022**, *44*, 4597–4613. [CrossRef]
16. Sousa, S.; Onofre, M.; Antunes, T.; Branco, C.; Maia, J.; Rocha, J.L.; Pires, V.F. Implementation of a low-cost data acquisition board for photovoltaic arrays analysis and diagnostic. In Proceedings of the 2013 International Conference on Renewable Energy Research and Applications (ICRERA), Madrid, Spain, 20–23 October 2013; pp. 1084–1088. [CrossRef]
17. Roncero-Clemente, C.; Romero-Cadaval, E.; Minambres, V.M.; Guerrero-Martinez, M.A.; Gallardo-Lozano, J. PV Array Emulator for Testing Commercial PV Inverters. *Elektron. Ir Elektrotehnika* **2013**, *19*, 71–75. [CrossRef]
18. Bun, L.; Raison, B.; Rostaing, G.; Bacha, S.; Rumeau, A.; Labonne, A. Development of a real time photovoltaic simulator in normal and abnormal operations. In Proceedings of the IECON 2011–37th Annual Conference of the IEEE Industrial Electronics Society, Melbourne, VIC, Australia, 7–10 November 2011; pp. 867–872. [CrossRef]
19. Kahoul, N.; Houabes, M.; Neçaibia, A. A comprehensive simulator for assessing the reliability of a photovoltaic panel peak power tracking system. *Front. Energy* **2015**, *9*, 170–179. [CrossRef]
20. Subsingha, W. Real-time Photovoltaic Simulator Using Current Feedback Control. *Energy Procedia* **2016**, *89*, 160–169. [CrossRef]
21. Tang, K.H.; Chao, K.H.; Chao, Y.W.; Chen, J.P. Design and Implementation of a Simulator for Photovoltaic Modules. *Int. J. Photoenergy* **2012**, *6*, 368931. [CrossRef]
22. Qi, H.; Bi, Y.; Wu, Y. Development of a photovoltaic array simulator based on buck convertor. In Proceedings of the International Conference on Information Science Electronics and Electrical Engineering, Sapporo, Japan, 26–28 April 2014; pp. 14–17. [CrossRef]
23. Cordeiro, A.; Foito, D.; Pires, V.F. A PV panel simulator based on a two quadrant DC/DC power converter with a sliding mode controller. In Proceedings of the International Conference on Renewable Energy Research and Applications (ICRERA), Palermo, Italy, 22–25 November 2015; pp. 928–932. [CrossRef]
24. Zhang, W.; Kimball, J.W. DC–DC Converter Based Photovoltaic Simulator with a Double Current Mode Controller. *IEEE Trans. Power Electro.* **2018**, *33*, 5860–5868. [CrossRef]
25. Chakraborty, I.; Sekaran, S.; Pradhan, S.K. An enhanced DC-DC boost converter based stand-alone PV-Battery OFF-Grid system with voltage balancing capability for fluctuating environmental and load conditions. *Energy Sources Part A Recovery Util. Environ. Eff.* **2022**, *44*, 8247–8265. [CrossRef]
26. Ahmad, R.; Murtaza, A.F.; Sher, H.A. Power tracking techniques for efficient operation of photovoltaic array in solar applications—A review. *Renew. Sustain. Energy Rev.* **2019**, *101*, 82–102. [CrossRef]

27. De Brito, M.A.; Galotto, L.; Sampaio, L.P.; e Melo, G.D.A.; Canesin, C.A. Evaluation of the Main MPPT Techniques for Photovoltaic Applications. *IEEE Trans. Ind. Electron.* **2013**, *60*, 1156–1167. [[CrossRef](#)]
28. Khodair, D.; Motahhir, S.; Mostafa, H.H.; Shaker, A.; Munim, H.A.E.; Abouelatta, M.; Saeed, A. Modeling and Simulation of Modified MPPT Techniques under Varying Operating Climatic Conditions. *Energies* **2023**, *16*, 549. [[CrossRef](#)]
29. Abo-Khalil, A.G.; El-Sharkawy, I.I.; Radwan, A.; Memon, S. Influence of a Hybrid MPPT Technique, SA-P&O, on PV System Performance under Partial Shading Conditions. *Energies* **2023**, *16*, 577. [[CrossRef](#)]
30. Asif, R.M.; Siddique, M.A.; Rehman, A.U.; Sadiq, M.T.; Asad, A. Modified Fuzzy Logic MPPT for PV System under Severe Climatic Profiles. *Pak. J. Eng. Technol.* **2021**, *4*, 49–55. [[CrossRef](#)]
31. Siddique, M.A.B.; Khan, M.A.; Asad, A.; Rehman, A.U.; Asif, R.M.; Rehman, S.U. Maximum Power Point Tracking with Modified Incremental Conductance Technique in Grid-Connected PV Array. In Proceedings of the 2020 5th International Conference on Innovative Technologies in Intelligent Systems and Industrial Applications (CITISIA), Sydney, Australia, 25–27 November 2020; pp. 1–6. [[CrossRef](#)]
32. Erickson, R.W.; Maksimovic, D. *Fundamentals of Power Electronics*, 2nd ed.; Springer: Berlin/Heidelberg, Germany, 2001; ISBN 978-0792372707.
33. Available online: https://www.pvxchange.com/Solar-Modules/JA-Solar/JAM60S21-365-MR_1-996000354 (accessed on 10 January 2023).
34. Asif, R.M.; Ur Rehman, A.; Ur Rehman, S.; Arshad, J.; Hamid, J.; Tariq Sadiq, M.; Tahir, S. Design and analysis of robust fuzzy logic maximum power point tracking based isolated photovoltaic energy system. *Eng. Rep.* **2020**, *2*, e12234. [[CrossRef](#)]
35. Soon, J.J.; Low, K.S. Optimizing Photovoltaic Model for Different Cell Technologies Using a Generalized Multidimension Diode Model. *IEEE Trans. Ind. Electron.* **2015**, *62*, 6371–6380. [[CrossRef](#)]
36. Gao, W.; Hung, J.C. Variable structure control of nonlinear systems: A new approach. *IEEE Trans. Ind. Electron.* **1993**, *40*, 45–55. [[CrossRef](#)]
37. Silva, J.F.; Pinto, S.F. Advanced Control of Switching Power Converters. In *Power Electronics Handbook*, 4th ed.; Rashid, H.M., Ed.; Butterworth-Heinemann: Oxford, UK, 2018; Chapter 35; ISBN 978-0128114070.
38. Ang, S.; Oliva, A.; Griffiths, G.; Harrison, R. *Power-Switching Converters*, 3rd ed.; CRC Press, Taylor & Francis Group: New York, NY, USA, 2011; ISBN 978-1439815335.
39. Pires, V.F.; Martins, J.F.; Hao, C. Dual-Inverter for Grid Connected Photovoltaic System: Modelling and Sliding Mode Control. *Sol. Energy* **2012**, *86*, 2106–2115. [[CrossRef](#)]
40. Mérida, J.; Aguilar, L.T.; Dávila, J. Analysis and synthesis of sliding mode control for large scale variable speed wind turbine for power optimization. *Renew. Energy* **2014**, *71*, 715–728. [[CrossRef](#)]
41. Pires, V.F.; Silva, J.F. Teaching nonlinear modeling, simulation, and control of electronic power converters using MATLAB/SIMULINK. *IEEE Trans. Educ.* **2002**, *45*, 253–261. [[CrossRef](#)]
42. PVSYST. 2022. Available online: <https://www.pvsyst.com/> (accessed on 10 January 2023).
43. Pvxchange. 2022. Available online: https://www.pvxchange.com/Solar-Modules/Schott-Solar/ASE-100-GT-FT-100W_1-992500269-1 (accessed on 10 January 2023).

Disclaimer/Publisher’s Note: The statements, opinions and data contained in all publications are solely those of the individual author(s) and contributor(s) and not of MDPI and/or the editor(s). MDPI and/or the editor(s) disclaim responsibility for any injury to people or property resulting from any ideas, methods, instructions or products referred to in the content.